The Thesis committee for Sean Stephen Bader
Certifies that this is the approved version of the following thesis:

Seismic and well log data integration using data-matching techniques

APPROVED BY

SUPERVISING COMMITTEE:

Sergey B. Fomel, Supervisor

Kyle T. Spikes

Carlos Torres-Verdín

Seismic and well log data integration using data-matching techniques

by

Sean Stephen Bader

THESIS

Presented to the Faculty of the Graduate School of

The University of Texas at Austin

in Partial Fulfillment

of the Requirements

for the Degree of

Master of Science in Geological Sciences

THE UNIVERSITY OF TEXAS AT AUSTIN

May 2018

Dedicated to my parents and grandparents who supported my education and provided encouragement over the years

Acknowledgments

I owe a great deal of gratitude to Dr. Sergey Fomel. He has provided me with the opportunity to continue my education in geophysics which is one of the most challenging, unique, and interesting fields of study. Sergey's insight and understanding of the theory and application of challenging geophysical concepts is unparalleled and has pushed me to broaden my horizons and understand the connections between concepts which I had thought were completely unrelated. He has allowed me the freedom to explore topics that I found interesting, and we tackled several fun and unique projects. I greatly appreciate everything Sergey has taught me during my time in Austin.

The work discussed in this thesis is an accumulation of several collaborations and publications. Each chapter is pieced together from the following works: Bader et al. (2017), Bader et al. (2018a), Bader et al. (2018b), Bader et al. (2018c), and Bader et al. (2018d). I am very thankful to the co-authors on these works in particular for their assistance and input on the projects.

The Texas Consortium for Computation Seismology (TCCS) has been home to me for the last two years, and the members of this group are kind, supportive and unbelievably hard working. I am very thankful to past and present members of the group that I have the opportunity to work with: Dr. Xinming Wu, Dr. Zhiguang Xue, Dr. Yanadet Sripanich, Dmitry Merzlikin, Yunzhi Shi, Mason Phillips, Luke Decker, Yunan Yang, Ben Gremillion, Zhicheng Geng, Harpreet Kaur, and Nam Pham. I also appreciate the financial support and insights provided by the sponsors of TCCS.

Additionally, I would like to thank Thomas Hess for advice and expertise on

processing and imaging techniques and the daily morning coffee. I also would like to thank Philip Guerrero who supports all of the geoscience graduate students at UT Austin. I appreciate the members of my committee, Kyle Spikes and Carlos Torres-Verdín for their feedback and recommendations on the work presented in this thesis.

Also, I am thankful for the many people whom I have had the opportunity to interact and work with since I started out at Colorado School of Mines, CO. During my undergraduate studies was unbelievably lucky to be surrounded by a group of friends and professors who are passionate about geology and geophysics and driven to succeed. I am especially thankful to Dr. Terence Young for introducing me to the field of geophysics; I would not have taken up this line of work without the guidance and support from him. Also, I want to thank Dr. Paul Sava and Dr. Thomas Davis who introduced me to the complexities of real-world problems in geophysics, and whose sense of humor reminded me to have fun solving these seemingly impossible problems.

I would also like to thank my sixth-grade teacher, Anne McIntosh, who introduced our class to higher levels of math and science that most elementary students do not get access to until later stages of school. Her approach to teaching and sense of humor set me up for many years of success.

I am very thankful to my grandparents, aunts, uncles and cousins who attended my various academic and sporting events confident that I will do great things. Of course, I might have gotten lost along the way if it were not for my Uncle Nate's multiple, lengthy, lectures about life in the car rides between Denver and Vail. Finally, I am deeply grateful to my loving parents, Marci and Jerry Bader, for their unwavering

support. Their love and constant encouragement pushed me to achieve new heights. And, last but not least, I am grateful for my siblings, Samantha and Andy, for putting up with me over the years.

Seismic and well log data integration using data-matching techniques

Sean Stephen Bader, M.S.Geo.Sci.

The University of Texas at Austin, 2018

Supervisor: Sergey B. Fomel

Relating well log data to seismic data is an important step in integrated reservoir characterization studies. Traditionally, an interpreter uses well log data, which has high vertical resolution but little lateral coverage, to understand amplitude variations in seismic data, which has lower vertical resolution than well logs but high spatial coverage. The process of calibration is referred to as a seismic-well tie.

Several problems arise with the assumptions of conventional seismic-well tie workflows. The seismic-well tie involves generating a reflectivity series from available sonic and density logs acquired at the well, which inherently assumes all wells have a sonic and density log available along the entire length of the well. In many cases, this assumption is not valid as the number of wells drilled often out-numbers the number of sonic and density logs acquired. Common procedures to account for missing well logs in seismic-well ties are to use a time-depth relationship from a nearby well or use an empirical relationship to estimate the missing well log from an avail-

able well log. These methods provide constructive solutions. However, variations in structure, stratigraphy or missing/incomplete well logs can result in inaccurate seismic-well ties. In this thesis, I propose a method that predicts missing well log data by first estimating the shifts that align well logs with a reference type log. Once in this stratigraphically correlated, or 'relative geologic time,' domain, I interpolate the missing well log data from available logs of the same type. The resulting well log is consistent with available well data and is not distorted by structural or stratigraphic variations. Once complete well log suites are estimated for each well, I focus on improving the efficiency and consistency of multiple seismic-well ties.

The seismic-well tie typically involves a subjective and labor-intensive workflow that depends on the interpreter's experience and intuition. I introduce an automatic workflow using local similarity to match the synthetic with the real seismic trace. The advantage of using local similarity to compute the seismic-well tie is that consistent, repeatable, seismic-well ties are achieved. I generate a global log property volume by interpolating log data along local seismic structure and perform blind well tests to verify the accuracy and consistency of seismic-well ties. I apply this workflow to a 3D seismic dataset with 26 wells and achieve consistent, accurate and reproducible seismic-well ties.

Combining the results of the well log interpolation and seismic-well tie I can generate a time-to-depth relationship for each well regardless of the initial well log suite. As a result, it is possible to generate log property volumes that integrate the high spatial coverage of seismic data with information from well log data.

Well log data can also provide a useful source of information during velocity model building for depth migration. Using concepts and workflows described previ-

ously, I show that the mis-tie between a modeled synthetic and real seismic trace is related to an inaccurate migration velocity. Furthermore, this information can be used to update the migration velocity model such that modeled synthetic seismograms, the seismic image, migration velocities and well log velocities become consistent.

Table of Contents

List of Figures

Chapter 1

Introduction

Oil and gas exploration in the United States has experienced a 'shale revolution' resulting in large increases in the total number of wells drilled onshore; it is expected that countries around the world will try to duplicate the United States' success (Morse, 2014). The focus on onshore exploration creates a unique challenge as companies rapidly accumulate more data to understand developing fields and discover new fields (Rashed, 2014). Furthermore, the speed at which onshore development occurs demands that datasets are analyzed efficiently and accurately to make timely drilling or business decisions. The development of methods and workflows that efficiently integrate well log and seismic datasets is a key to quickly uncover subsurface rock-property distributions. My research focused on developing methods and workflows based on automatic data matching techniques that can be used as tools for efficiently and accurately linking well log data to seismic data.

Effective exploration and exploitation of hydrocarbon resources involves careful integration of multiple datasets in an attempt to understand the distribution of subsurface rock properties. One of the most practical data integration techniques is the seismic-well tie: where well logs are used to calibrate lower resolution seismic data, while seismic data are used to spread information from well logs. White and Simm (2003) discuss the seismic-well tie procedure as a series of steps:

1. Edit and calibrate sonic and density logs.

2. Construct the appropriate reflection series in two-way time.

3. Perform the match.

4. Validate the approach.

Each step can be challenging and ambiguous. If the results of seismic-well tie are accurate, the interpreter can verify that tops picked from well log data relate to a reflector that can be interpreted in a seismic dataset. Integrating well log and seismic data in this way is a key step in velocity model building, post-stack seismic interpretation and pre-stack seismic inversion. For these reasons, accurate calibration of seismic data with well log data continues to be the foundation for integrated reservoir studies in exploration geophysics.

In the first part of this thesis, I focus on each step in the conventional seismic-well tie procedure and propose alternative methods and workflows that provide more efficient, accurate and repeatable results. I present an approach that uses the data matching techniques, local similarity (LSIM) and predictive painting, to estimate missing sonic and density well logs, automatically tie synthetic seismograms to observed seismic traces, and interpolate all available well log data along seismic structure to validate results. The well log estimation and seismic-well tie approaches utilizes LSIM, which estimates local shifts to align two datasets, making the method especially useful in correlating geologic datasets where structural and stratigraphic variations may be prevalent (Fomel, 2007a). I use LSIM with hard and soft constraints to align several well logs to relative geologic time (RGT) using a type log as reference for well

log alignment. In this aligned domain, which is analogous to a stratigraphic correlation, I interpolate missing well log data assuming fluid variations have a negligible effect on the well logs and the reference well log is representative of the entire stratigraphic column. Finally, I use LSIM to iteratively align synthetic seismiograms with real real seismic traces. Unlike the conventional manual approaches to relate well log data to seismic data, my approach is not limited to wells with specific well log suites, can consistently and accurately tie wells to seismic data and provide a method for validation.

In the second part of this thesis, I discuss a novel approach to updating migration velocity models using seismic-well tie results. Seismic migration uses geophysical velocities to properly place dipping reflectors and diffracted energy in the seismic image. Inaccuracies in seismic migration velocities may result in reflector timings that are inconsistent with a synthetic seismogram modeled from well log data (White et al., 1998b). The resulting seismic-well tie will warrant a correction. Although this correction is often in the form of an updated velocity log, it can be used as an update to the seismic migration velocity. I construct several experiments to test this hypothesis and using similar approaches as discussed in the first part of the thesis, I show that a mis-tie from seismic-well ties can indeed be applied as a tool to update the migration velocity model which improves the seismic image.

THESIS OUTLINE

In Chapter 2, I review several steps of the seismic-well tie procedure mentioned previously and conventional methods used to complete each step. In cases where sonic or density logs are missing, I discuss several previously proposed empirical estimations for predicting missing well log data and challenges that arise with

the assumptions behind each estimation. Additionally, I consider several previously proposed approaches that aim to improve the efficiency and accuracy of multiple seismic-well ties. Next, I introduce several novel approaches for interpolating data along seismic structure, which both aid the interpreter in understanding subsurface rock-property distributions and provides a method to validate seismic-well ties. Finally, I review the LSIM method, which is a regularized local correlation method that serves as the key tool for the methods and workflows I propose in later chapters.

In Chapter 3, I use a gamma log, acquired at every well location in a 3D dataset, and the LSIM method to estimate shifts that align all logs to a common relative geologic time (RGT). I then use the aligned well logs to predict missing well log data by solving the least-squares problem to effectively interpolate missing data from other well logs of the same type. Finally, I attempt to improve upon the method by including empirical estimations that relate velocity, density and porosity to predict the missing log data using a Bayesian approach. The predicted velocity and density well logs provides the minimum required logs to forward model a synthetic seismogram and tie the well with real seismic data assuming no changes in fluids between wells and the type log is representative of the entire stratigraphic column.

In Chapter 4, I discuss using LSIM to automatically perform the seismic-well tie matching procedure. I also discuss the theory behind using the estimated shifts to update the well velocity log. I introduce a soft constraint to the LSIM method that accounts for the energy of the synthetic seismogram and seismic trace to improve the matching. Finally, using the results from Chapter 3 and the automatic seismic-well tie workflow, I show that accurate time-to-depth relationships can be estimated for each well, regardless of the initial well log suite.

In Chapter 5, I use the results from the previous chapters to qualitatively asses seismic-well ties by interpolating well log data along local seismic dip using predictive painting. Using the volumes of log properties, I quantitatively asses results by performing blind well tests to compare the interpolated log against the actual log at test well location.

In Chapter 6, I construct controlled experiments to show that the mis-tie between a synthetic seismogram modeled from well log data and a seismic image can be related to an incorrect migration velocity. Using approaches proposed previously, I show that mis-tie information can be used to update the migration velocity model, which in turn improves the seismic image. This process results in achieving consistency between modeled synthetic seismograms, the seismic image, well log velocity profiles and the migration velocity.

In Chapter 7, I conclude this thesis with a brief summary and discussion of the results. I discuss the advantages and disadvantages of the methods and workflows introduced in this thesis and consider several potential future applications of this work in exploration geophysics.

Chapter 2

Review

In this chapter, I discuss concepts and limitations behind conventional seismic-well tie procedures. This discussion includes methods that predict missing well log data as well as previously proposed methods for estimating automatic seismic-well ties. I also review several approaches for interpolating data along seismic structures, which are used as a validation technique in later chapters. I introduce the local similarity method (LSIM), which is a regularized local correlation method that serves as the key tool for the methods and workflows I propose in later chapters. Finally, I discuss previously proposed approaches for using well log data in migration velocity model building.

SEISMIC-WELL TIE PROCEDURE: KEY CHALLENGES AND PREVIOUSLY PROPOSED SOLUTIONS

Oil and gas exploration involves careful integration of multiple datasets in an attempt to understand the distribution of subsurface rock properties. One common approach to integrating multiple datasets is the seismic-well tie: where well logs are used to calibrate lower resolution seismic data. This calibration, often referred to as a 'seismic-well tie' is critical to using seismic data for predicting fluid and lithological properties away from the well (White et al., 1998a). The seismic-well tie involves estimating a synthetic seismogram that is typically based on the one-

dimensional convolutional model. Assuming zero noise, a synthetic seismogram, $s(t)$ is the convolution of the earth's reflecitivity series, $r(t)$ with a seismic source, $w(t)$ (Russell, 1988):

$$s(t) = r(t) * w(t). \tag{2.1}$$

To estimate the earth's reflectivity series as a function of time, one starts with the acoustic impedance as a function of depth, $I(z)$, which is the product of compressional velocity, $v(z)$, and density, $\rho(z)$:

$$I(z) = v(z)\rho(z). \tag{2.2}$$

The seismic source is sensitive to changes in impedance, or reflectivity; mathematically, the normal reflectivity is the difference in acoustic impedances divided by the sum of acoustic impedances between two layers (White and Simm, 2003).

$$r(z) = \frac{I(z + \Delta z) - I(z)}{I(z + \Delta z) + I(z)}. \tag{2.3}$$

The estimation of reflectivity in depth from well log data is shown in Figure 2.1 using data from Penobscot L-30 well offshore Nova Scotia, Canada (Bianco, 2014). Interpolating Equation 2.3 from depth to time requires a time-to-depth relationship (TDR). There are several ways to compute a TDR. Using available checkshot surveys or vertical seismic profiles (VSP) can provide accurate measurements of seismic travel times to known depths; however, these surveys are not always available (White and Simm, 2003). An alternative approach is integrating the sonic log transit times:

$$T(z) = 2 \int_{z_{min}}^{z} \frac{d\xi}{v(\xi)}, \tag{2.4}$$

where $T(z)$ is the TDR are each depth, z_{min} is the minimum depth at which acoustic velocity information is available, and dz is the depth increment. The TDR can be

used to effectively interpolate the reflectivity series to time:

$$r(t) = r(T(z)). \tag{2.5}$$

The reflectivity series in time is then filtered with a seismic source to generate a synthetic seismogram as discussed in Equation 2.1. Using the velocity profile shown in Figure 2.1, I estimate a TDR to interpolate reflectivity from depth to time. The resulting reflectivity profile is convolved with a 25Hz Ricker wavelet to generate a synthetic seismiogram in Figure 2.2.

The one-dimensional convolutional model assumes normal incidence. In cases where this assumption reduces the quality of a seismic-well tie, there are several alternative approaches. One option is the Zoeprittz Equation or an approximation of the Zoeppritz Equation which generate reflectivity as a function of angle of incidence (Aki and Richards, 2002; Shuey, 1985). In cases where internal multiples and mode conversions must be considered another option is to model the reflectivity elastically. Muñoz and Hale (2015) use the propagator matrix method for vertically propagating plane waves in stratified media to model these complex effects (Kennett, 1986). Each method assumes stratified media and may provide a reflectivity series that is more representative of the earth's reflectivity series as compared to one-dimensional convolution. For the purposes of this thesis, I use simple one-dimensional convolution to estimate all synthetic seismograms.

Using the synthetic seismogram, I compare the modeled waveforms to real seismic data in Figure 2.3. This comparison helps the interpreter to understand how well log data and interpreted well facies relate to the seismic data. Using this understanding, it is possible to use the seismic data to gain a 3D understanding of structural, stratigraphic and potentially rock property distributions of the subsurface.

Bianco (2014) observes that to align the synthetic seismogram and real seismic data in Figure 2.3, a bulk shift can be applied to align the waveforms in the synthetic seismogram with the seismic data.

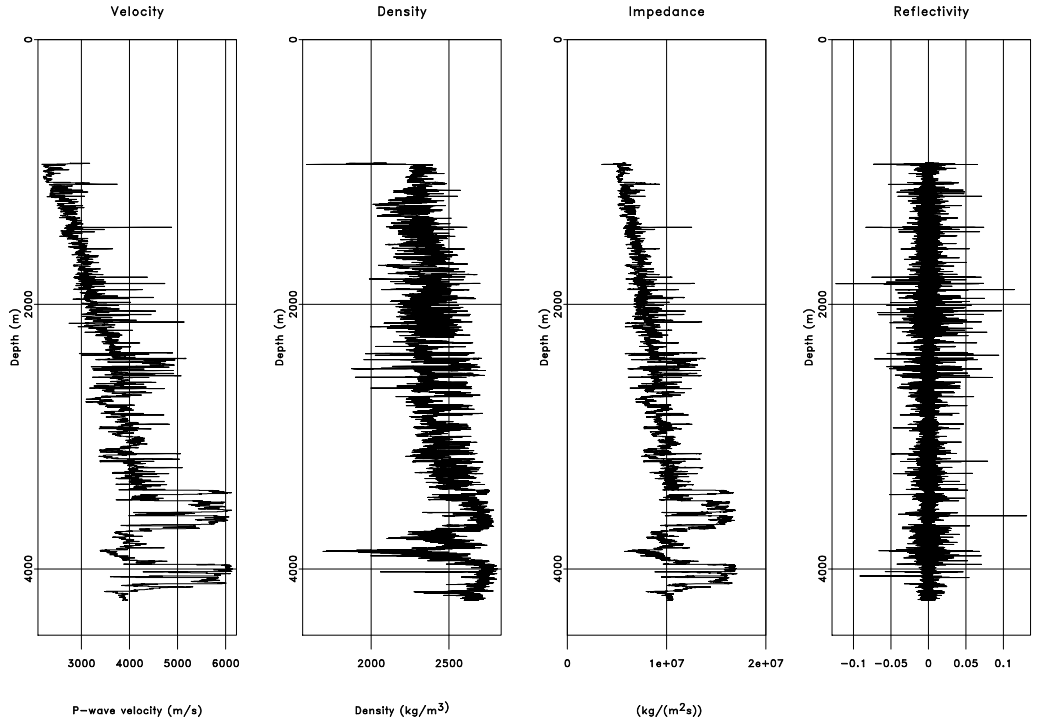

Figure 2.1: Example estimating impedance and reflectivity from well log data. The velocity and density data are from the Penobscot L-30 well offshore Nova Scotia, Canada. ch02-review/smpltie logs

The progression illustrated in Figures 2.1, 2.2, and 2.3 represents an idealized scenario where the velocity well log, density well log and seismic data are available. The well logs contain no missing section, and the forward modeled waveforms are consistent with real seismic data. In many cases, missing sonic or density logs can make it challenging or impossible to generate a reflectivity series that is representative of the well log data. A missing sonic log proves to be a significant challenge as it is crucial for generating a TDR. Furthermore, inaccuracies in seismic migration models

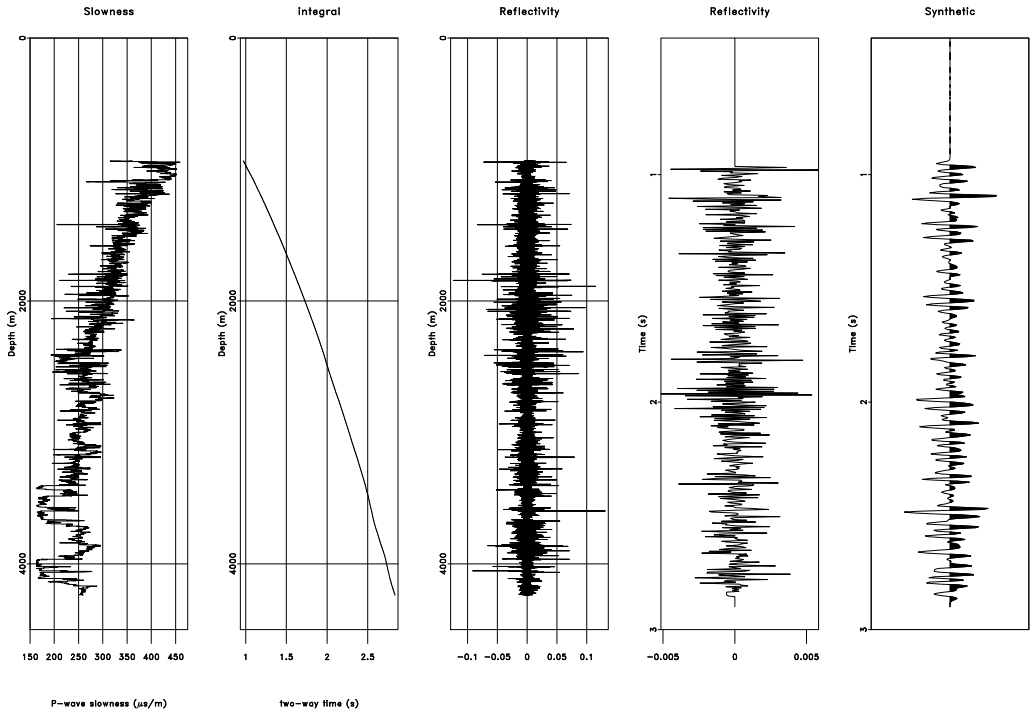

Figure 2.2: Example estimating a time-to-depth relationship using a well log velocity profile. Reflectivity in depth is interpolated to time using the time-to-depth relationship and convolved with a 25Hz Ricker wavelet to generate a synthetic seismogram. The velocity and density data are from the Penobscot L-30 well offshore Nova Scotia, Canada. ch02-review/smpltie logst

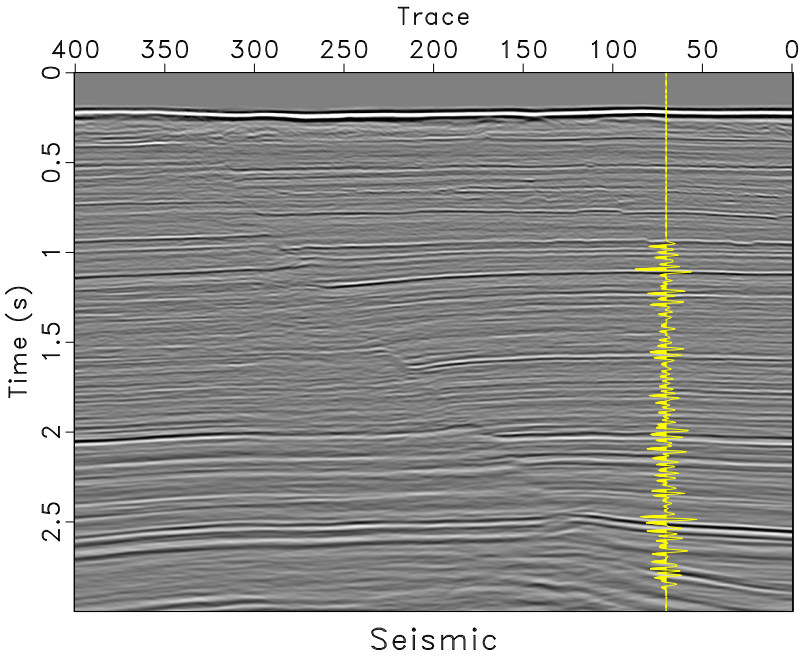

Figure 2.3: Synthetic seismogram modeled from well log data overlaying seismic amplitude data. The velocity and density data are from the Penobscot L-30 well and seismic data are from a dataset offshore Nova Scotia, Canada. ch02-review/smpltie seismic2

will cause a mistie between the waveforms modeled in a synthetic seismogram and real seismic data (White et al., 1998b).

Missing well log data prediction methods

Several approaches have been proposed to predict missing well log data. I will focus, in particular, on methods pertaining to predicting missing sonic and density logs as these logs are vital for modeling a synthetic seismogram and a seismic-well tie. A simple linear interpolation of missing log data between wells allows for estimation of a reflectivity series and TDR; however, this method does not account for variations in lithology or structure, so applying a TDR generated at one well to a nearby well may result in a mis-tie with the seismic data. In Figure 2.4, I remove a 1500ft interval of sonic log from the previous example. The resulting reflectivity series and modeled synthetic seismogram has a gap due to the missing sonic log, which may make it challenging to relate to the available seismic data.

Alternatively, several approaches are based on empirically derived relationships between one well log type and a different well log type. Gardner's Equation has been shown to provide a reasonable relationship between sonic and density well logs data for a large number of brine saturated rock types (Gardner et al., 1974).

$$\rho_b = \alpha v_p^{\beta}. \tag{2.6}$$

where

$$v_p = \text{P-wave velocity in } \frac{ft}{s}$$

$$\rho_b = \text{Bulk density from log in } \frac{g}{cm^3}$$

$$\alpha = \text{Constant} \approx 0.23$$

$$\beta = \text{Constant} \approx 0.25$$

Using the previous example, I crossplot the available density and velocity data as well as Equation 2.6 in Figure 2.5. Gardner's equation is a reasonable representation of the available log data; however, the parameters α and β should be estimated for each stratigraphic interval; I will return to this understanding in chapter 3, where I propose to estimate missing well log data in the relative geologic time domain using Bayes' Theorem. Using Equations 2.6, I estimate the missing section of sonic log shown in Figure 2.4 from the available density log. Results of this process are shown in Figure 2.6. The resulting synthetic seismogram may be a better representation of the subsurface at that location and does not have a gap due to missing information.

Additionally, in wells where a resistivity log is acquired, the Faust method and Smith method provide empirical relationships between resistivity and sonic well logs (Faust, 1953; Smith, 2007). Alternatively, if there is a high interdependence of different well log types but the relationship is not inherently clear, Saggaf and Nebrija (2003) apply regularized back-propagation neural networks to estimate missing portions of sonic logs. Each empirical relationship may provide a useful approximation to a missing log; however, each method assumes that required logs are collected at every well location to carry out the estimation.

An alternative approach is to assume that rock properties do not vary signifi-

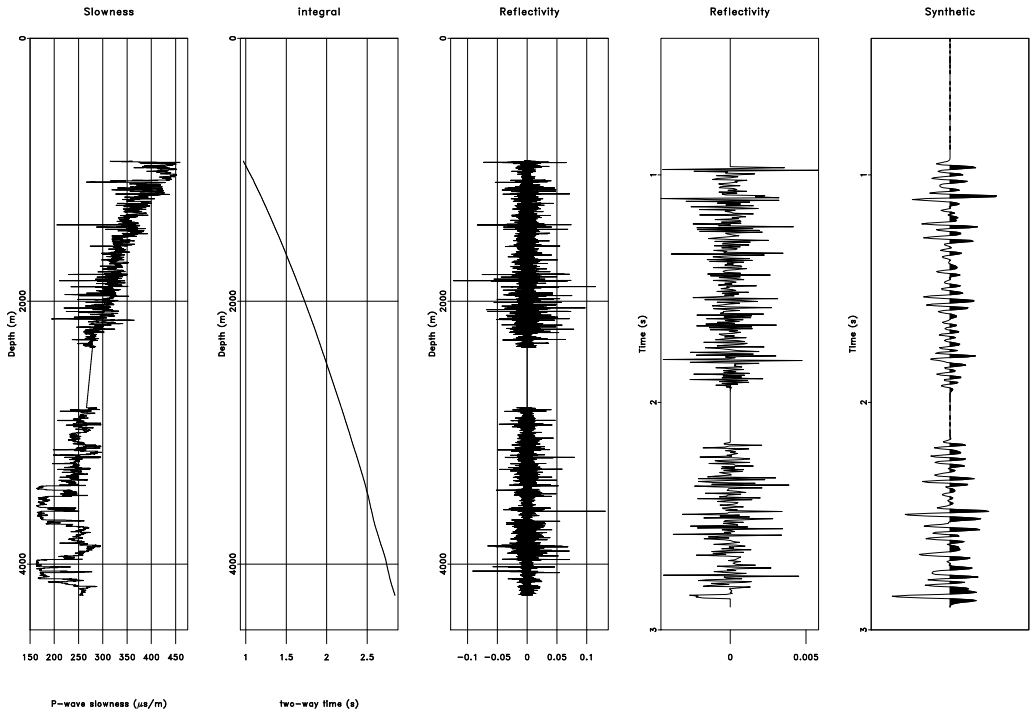

Figure 2.4: Example using linear interpolation to fill in the missing sonic log data. Using the resulting sonic log, a synthetic seismogram can be modeled; however, a gap is present due to the missing sonic log, which may make it challenging to relate to the available seismic data. ch02-review/smpltie logstmi

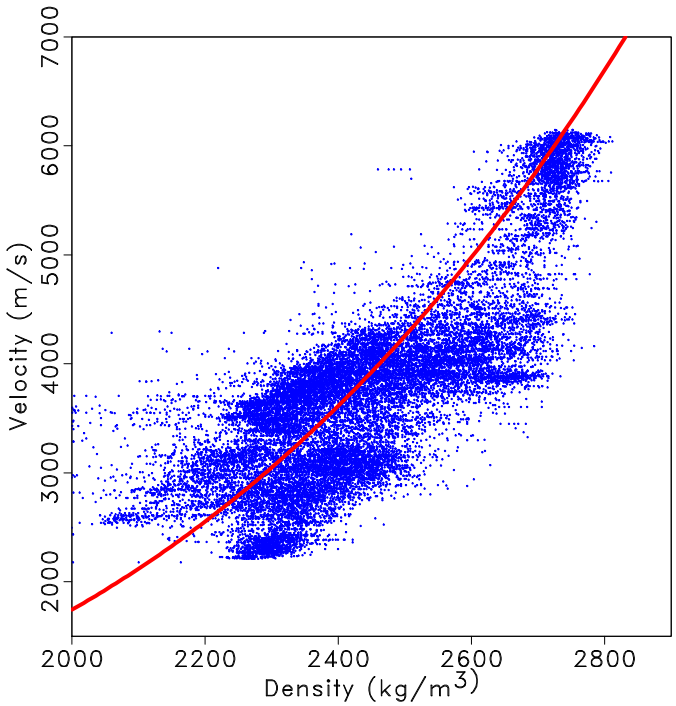

Figure 2.5: Crossplot of velocity and density log data from the Penobscot L-30 well. Using Gardner's Equation, I relate the available sonic and density log data assuming $\alpha = 0.23$ and $\beta = 0.25$ for the entire well. ch02-review/smpltie xplot-gard

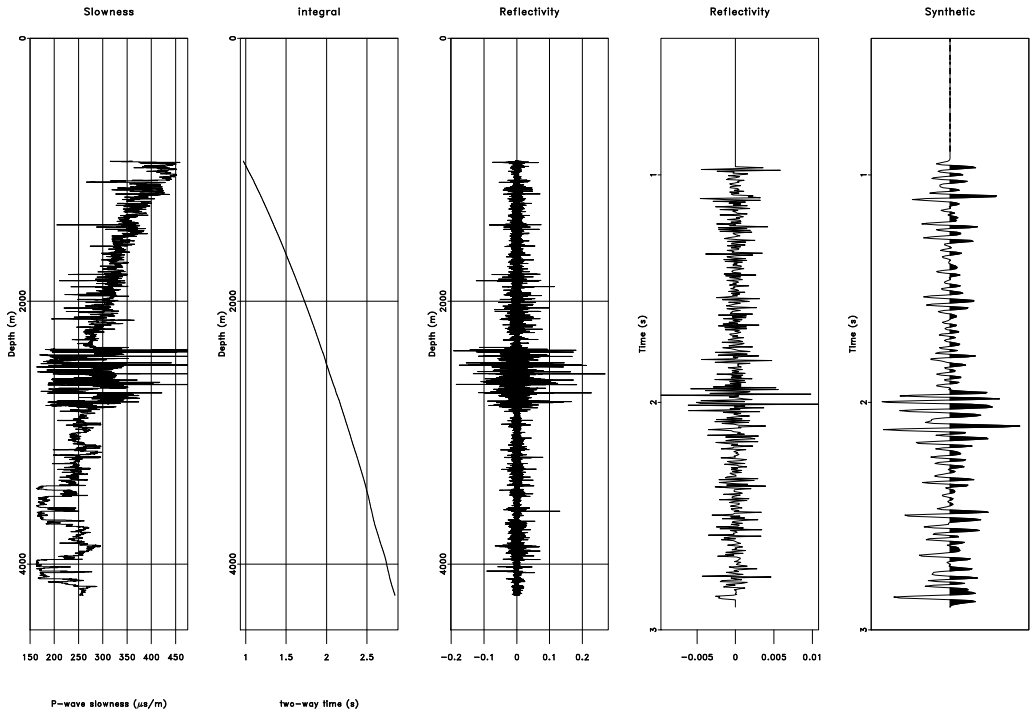

Figure 2.6: Example using Gardner's Equation to fill in the missing sonic log data. Using the resulting sonic log, a synthetic seismogram can be modeled that might be a better representation of the subsurface at that location and does not have a gap due to missing information. ch02-review/smpltie logstgard

cantly in lateral space, which allows density and sonic logs from a nearby well to be used to estimate a TDR. This assumption does not take into consideration structural or stratigraphic variations in lithology. To account for these variations, the well must be correlated to a constant geologic time, which is analogous to stratigraphic correlation. Wheeler and Hale (2014) and Wu et al. (2017) use dynamic time warping (DTW) (Berndt and Clifford, 1994; Hale, 2013) to correlate multiple well logs. Shi et al. (2017b) use local similarity scan (LSIM) (Fomel, 2007a) to optimally sort and flatten multiple well logs. This well log correlation is analogous to a stratigrahpic correlation and may be convenient for stratigraphically constrained operations such as normalization. I will return to this observation in Chapter 3, where I propose to estimate missing well log data in the relative geologic time domain.

Automatic seismic-well ties

The manual seismic well tie involves matching common reflectors between modeled synthetic and seismic data by stretching and squeezing the synthetic until a desired correlation between the datasets is achieved (White and Simm, 2003). This procedure is a subjective, labor-intensive workflow that strongly depends on the interpreter's experience and intuition. To reduce the interpreter bias and improve consistency among multiple seismic well ties, several automatic methods have been proposed. Muñoz and Hale (2012) use DTW to automatically align real and synthetic seismograms; this approach is extended to automatically and simultaneously tie multiple wells to seismic data by estimating a synthetic image to tie with the seismic image ensuring lateral consistency of the well ties (Muñoz and Hale, 2015). Further, Wu and Caumon (2017) show that laterally consistent seismic well ties are achieved by using DTW to correlate synthetic and seismic data that are 'flattened'

to constant relative geologic time. An alternative approach to carry out the seismic well tie is LSIM; Herrera et al. (2014) compare DTW with LSIM, showing that both methods can successfully compute a seismic well tie. Their study shows that using DTW can achieve a higher correlation between synthetic and seismic data compared to LSIM; however, the resulting TDR using DTW shows an oscillatory behavior due to stretching and squeezing.

Interpolation along seismic structure

Once each well is tied to the seismic data, the high spatial coverage of seismic data can be utilized to understand lateral variations in log properties and check the consistency of seismic-well ties. Muñoz and Hale (2015) show that when wells are improperly tied to seismic data, there can be a qualitative mis-match in a well log interpolated cross section between wells. Several methods have been proposed to interpolate log data along local seismic structures. Assuming available log data is properly tied to a nearby seismic trace and conforms to seismic image features, Hale (2010) uses image-guided blended-neighbor interpolation (Hale, 2009) for seismically guided well log interpolation. Alternatively, Karimi et al. (2017) show that predictive painting (Fomel, 2010) can be used to interpolate log data along seismic structures to generate accurate starting models for post stack inversion. Fomel (2016) presents a fast interpolation algorithm for interpolating scattered data to a regularly sampled grid. Interpolation along seismic structure using well log data generates log property volumes that conform to both well log and seismic datasets. Wu (2017) proposes to compute such a structurally conformable model in the flattened space, where the seismic data is first unfaulted and unfolded, then well log data are interpolated in the flattened domain. After interpolating the well log data, the model is returned to the

original domain.

In this thesis, I adopt predictive painting to interpolate well log data along seismic structure. Predictive painting is defined using plane-wave destruction filters that measure the local slopes of seismic events (Fomel, 2002). The plane-wave destruction operator can be written in linear operator notation

$$\boldsymbol{r} = \boldsymbol{D}\boldsymbol{s} \tag{2.7}$$

where $\mathbf{s}$ is a group of seismic traces from a seismic image ($\mathbf{s} = [\mathbf{s}_1\mathbf{s}_2...\mathbf{s}_N]^T$), $\mathbf{r}$ is the destruction residual, and $\boldsymbol{D}$, the destruction operator, is defined as

$$\boldsymbol{D} = \begin{bmatrix} \boldsymbol{I} & \mathbf{0} & \mathbf{0} & \dots & \mathbf{0} \\ -\boldsymbol{P}_{\mathbf{1,2}} & \boldsymbol{I} & \mathbf{0} & \dots & \mathbf{0} \\ \mathbf{0} & -\boldsymbol{P}_{\mathbf{2,3}} & \boldsymbol{I} & \dots & \mathbf{0} \\ \vdots & \vdots & \vdots & \ddots & \vdots \\ \mathbf{0} & \mathbf{0} & \dots & -\boldsymbol{P}_{\boldsymbol{N-1,N}} & \boldsymbol{I} \end{bmatrix} \tag{2.8}$$

where $\boldsymbol{I}$ is the identity operator and $\boldsymbol{P}_{\boldsymbol{i,j}}$ describes the prediction of trace $\mathbf{j}$ from trace $\mathbf{i}$ by shifting along the local slope of the seismic data. Slopes can be estimated in this way by minimizing the prediction residual operator $\mathbf{r}$ using regularized least-squares optimization. The prediction of one trace from another trace (Fomel, 2010) can be defined as

$$\boldsymbol{s}_{\boldsymbol{k}} = \boldsymbol{P}_{\boldsymbol{r,k}}\boldsymbol{s}_{\boldsymbol{r}} \tag{2.9}$$

where $\boldsymbol{s}_{\boldsymbol{k}}$ is the unknown trace and $\boldsymbol{s}_{\boldsymbol{r}}$ is the reference trace. The predictive painting operator is defined as:

$$\boldsymbol{P}_{\mathbf{1},\boldsymbol{k}} = \boldsymbol{P}_{\boldsymbol{k-1,k}} \dots \boldsymbol{P}_{\mathbf{2,3}}\boldsymbol{P}_{\mathbf{1,2}} \tag{2.10}$$

Predictive painting spreads information along local seismic structures to generate volumes of well log data from a single well log reference trace providing a method to predict an expected log profile in a location with no well log data.

Additionally, Karimi et al. (2017) show that several well logs can be combined by weighting the interpolation based on the lateral distance from the reference well as defined by a radial basis function (RBF) (Powell, 1985). The RBF has a higher weight for distances closer to the well location as compared to farther away. The RBF can be combined with interpolated log property volumes generated from data at each well location using the following interpolant:

$$\boldsymbol{V(x)} = \frac{\sum_{\boldsymbol{k}}^{\boldsymbol{N}} \boldsymbol{\phi}(|\boldsymbol{x} - \boldsymbol{x_k}|)\boldsymbol{S_k(x)}}{\sum_{\boldsymbol{k}}^{\boldsymbol{N}} \boldsymbol{\phi}(|\boldsymbol{x} - \boldsymbol{x_k}|)} \tag{2.11}$$

where $\boldsymbol{S_k}$ is the volume created by spreading log data from location $\boldsymbol{x_k}$ to the entire seismic data set using predictive painting weighted by the RBF, $\boldsymbol{\phi(m)}$, and $\boldsymbol{N}$ is the total number of wells used in the interpolation. Recently, Shi et al. (2017a), propose an approach that combines the RBF with the distance along seismic structure to weight the interpolation providing a more intuitive weighting scheme as compared to weighting based only on lateral distance from the well.

LOCAL SIMILARITY METHOD*

The workhorse behind many of the proposed methods in this thesis is the local similarity method (LSIM), which is a data matching technique. Matching datasets involves aligning similar waveforms between two datasets. Whether aligning two logs from different wells or aligning a modeled synthetic seismogram with a seismic trace, I focus on matching a response that corresponds to similar lithologies between the two datasets or a constant geologic time. In comparing two datasets, the purpose is to estimate a smoothly varying warping function, $\boldsymbol{S_k}$, required to align one dataset, $\boldsymbol{h_k}$, to a reference dataset, $\boldsymbol{r_k}$,

*Parts of this section are published in Bader et al. (2018c).

$$r_k(t) \approx h_k(S_k(t)) \tag{2.12}$$

I can represent the warping function with the shifts, $g_k(t)$, as follows:

$$S_k(t) = t + g_k(t) \tag{2.13}$$

where the t denotes the original independent axis and $g_k(t)$ are the shifts required to match the datasets as defined in Equation 2.12. The correlation coefficient can be used to quantify the quality of the match between datasets (Hampson-Russell, 1999). The LSIM method begins with the observation that the correlation coefficient (c) only provides one number to describe the datasets; however, I am interested in understanding the local changes in the datasets' similarity. Therefore, the LSIM method computes local similarity c_t, which is a function of time, t. The square of c can be split into a product of two factors (Fomel, 2007a):

$$c_t^2 = r_t * h_t \tag{2.14}$$

where r_t and h_t are the solutions to the following regularized least-squares problems, respectively

$$\min_{r_t}(\sum_t (a_t - r_t b_t)^2 + R[r_t])$$
$$\min_{h_t}(\sum_t (b_t - h_t a_t)^2 + R[h_t])$$

The regularization operator, R, is implemented using shaping regularization (Fomel, 2007b) and designed to enforce smoothness. To estimate the solution, LSIM is calculated for a series of shifts. The results of this calculation are accumulated and displayed on a 'similarity scan' as shown in Figures 2.9 and 2.11 in the following

synthetic example. From the similarity scan, I select the series of shifts along the entire length of the reference dataset that optimally aligns the two datasets (Fomel and Jin, 2009).

To illustrate the alignment of two datasets using local similarity, I use two examples based on the simple model shown in Figure 2.7. In our first example, I apply a 40ms shift to the modeled synthetic seismogram and use LSIM to estimate the shifts to realign the shifted synthetic model with the original synthetic model (Figure 2.8). Estimation of the shifts for the first example is visualized in a local similarity scan shown in Figure 2.9. In our second example, I add 15% random noise to the reflectivity model and convolve the noisy reflectivity with a 30Hz Ricker wavelet to create a noisy reference trace. LSIM is used to estimate the shifts to realign the shifted synthetic model with the noisy reference trace in Figure 2.10. Estimation of the shifts for the second example is visualized in a local similarity scan shown in Figure 2.11. From our synthetic examples, I observe that shifts can be accurately estimated to align a modeled seismogram with both a noise-free and noisy reference seismograms.

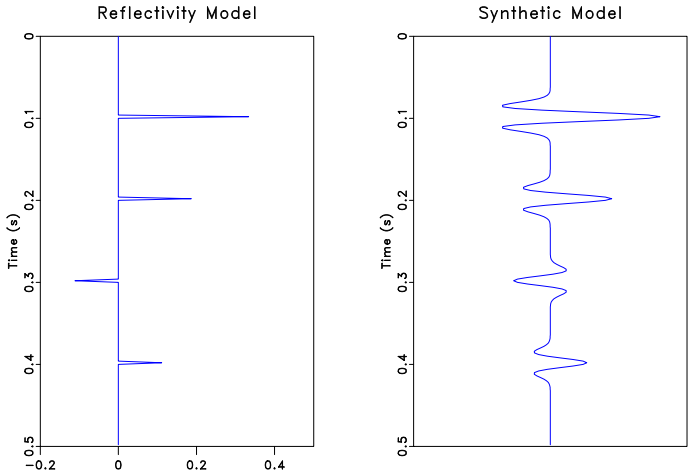

Figure 2.7: Reflectivity series in time (left) convolved with a 30Hz Ricker wavelet to model a seismogram (right). ch02-review/synthetic-example modelb

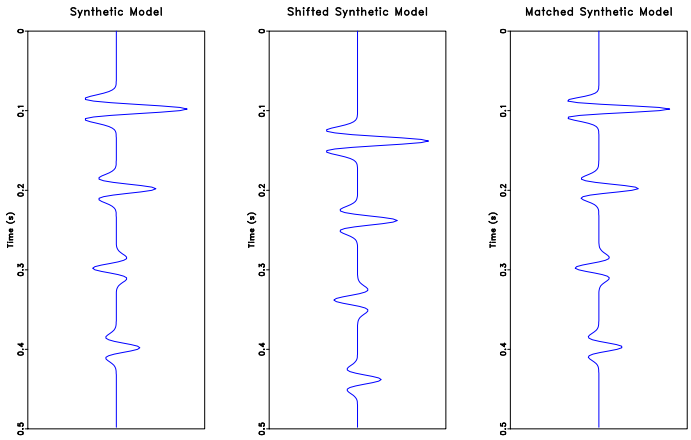

Figure 2.8: Modeled seismogram (left), modeled seismogram shifted by 40ms (middle), re-aligned seismogram using the shifts estimated from the local similarity scan (right). ch02-review/synthetic-example shifted-matched

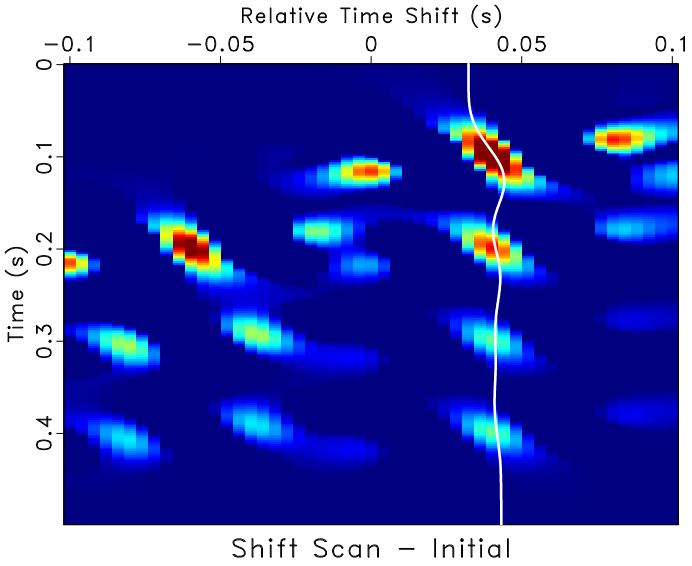

Figure 2.9: Similarity scan and picked optimal shifts (white curve). Warm colors represent high similarity whereas cool colors represent low similarity. ch02-review/synthetic-example scanch2

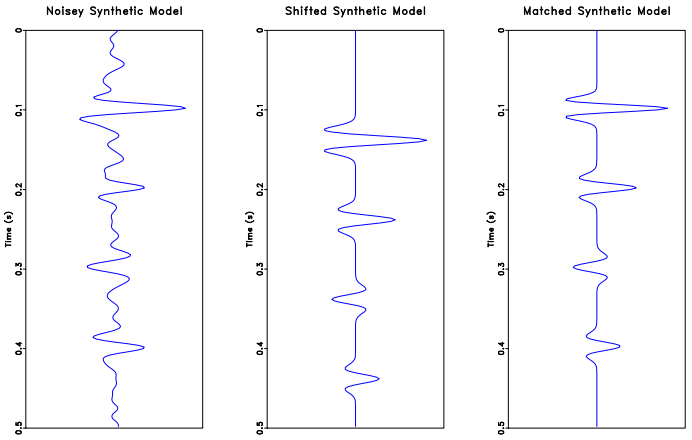

Figure 2.10: Noisy reference trace (left), modeled seismogram shifted by 40ms (middle), re-aligned seismogram using the shifts estimated from the local similarity scan (right). ch02-review/synthetic-example noise-matched

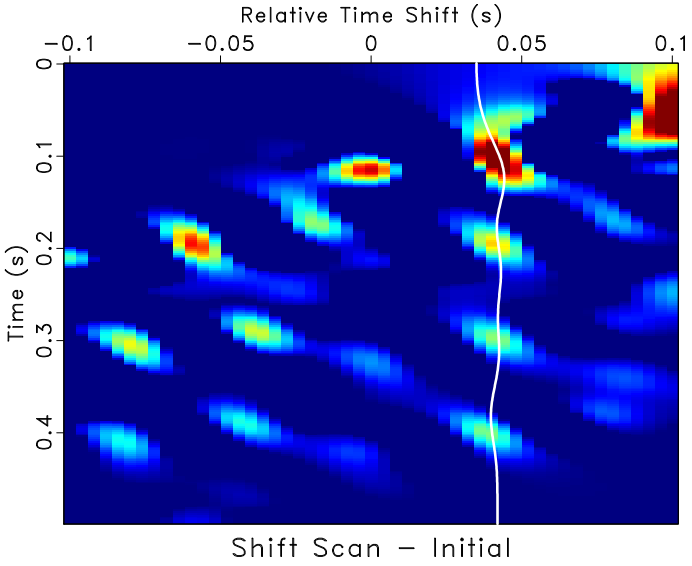

Figure 2.11: Similarity scan and picked optimal shifts (white curve). Warm colors represent high similarity whereas cool colors represent low similarity. ch02-review/synthetic-example scan-noise

WELL LOGS AND VELOCITY MODEL BUILDING

Mis-ties between the modeled synthetic seismograms and seismic data can be used to update the well's TDR and explained by inaccuracies in either the seismic phase or seismic migration velocities (White et al., 1998b; Henry, 2000). I will focus on the relationship between inaccuracies in the seismic migration model and the resulting seismic well tie mis-tie. In an attempt to reduce the mis-tie between well log information, which is taken as the ground truth, and the seismic image, well log measurements can be injected into migration velocity model building to provide constraints in an otherwise non-unique problem (Bakulin et al., 2010). Morice et al. (2004) show that combining well log, borehole and surface seismic data can provide an understanding of seismic velocities, anisotropy, attenuation and interbed multiples, and can further aid in building a velocity model consistent between all datasets.

Egozi et al. (2006) show that mis-tie surfaces generated from multiple picks in multiple wells can be used to iteratively update a TTI velocity field thus driving the cumulative average mistie of all wells towards zero. Using well marker-related workflows in velocity model building removes or reduces non-uniquness and may allow for simultaneous estimation of velocity and anisotropy parameters which can be used to constrain tomography problems that focus on flattening the residual moveout of seismic events (Woodward et al., 2008; Bakulin et al., 2010). Although, well marker-related workflows help integrate well log interpretations with seismic velocity model building; these methods are limited to updates related to only discrete pre-selected well markers.

The literature referenced above is by no means exhaustive; however, the workflow for including 'well data' is consistently based on the tomography principle using the depth mismatch between tops selected in logs and depth seismic interpretations. Beyond short discussions by White et al. (1998b) and the relationship between the mis-tie and velocity well log update (Muñoz and Hale, 2015; Herrera et al., 2014), there is little discussion in the literature about the interpretation of mis-ties in isotropic and anisotropic media. This general lack of understanding clouds the relationship between well log velocity, migration velocity, synthetic seismograms and seismic data, which should ideally be interpreted in a consistent way.

Chapter 3

Missing Log Data Estimation

In plays where the number of wells drilled outnumbers the number of sonic and density logs acquired, estimating missing logs is an essential step to understand how changes observed in well logs relate to amplitude variations in seismic data. I estimate a complete sonic log using all other sonic logs in the dataset and compare it against the actual sonic log from the well. These results are also compared against Reverse Gardner's equation for estimating missing sonic logs. I then extend the approach to honor true well log values for well logs that have incomplete or partial well logs.

There are several potential sources of information that can be used to constrain the estimation of missing log data: (1) the same well log type at other well locations, (2) other well logs within the same well, and (3) the seismic data. In the first section, I focus on using other well logs of the same type type in our estimation of a missing log. In the second section, I extend the approach to include models that relate different well log types and uncertainty to estimate a missing log using Bayes' Theorem.

Missing log data interpolation*

*Parts of this section are published in Bader et al. (2018c) and Bader et al. (2018d).

In this section, I focus on using other well logs of the same type in our estimation of a missing log. Generally, we include information from all other wells in our estimation:

$$\begin{bmatrix} \boldsymbol{W_1} \\ \boldsymbol{W_2} \\ \vdots \\ \boldsymbol{W_N} \end{bmatrix} \tilde{\boldsymbol{l}} \approx \begin{bmatrix} \boldsymbol{W_1}\hat{\boldsymbol{l_1}} \\ \boldsymbol{W_2}\hat{\boldsymbol{l_2}} \\ \vdots \\ \boldsymbol{W_N}\hat{\boldsymbol{l_N}} \end{bmatrix} \tag{3.1}$$

where our estimated log, $\tilde{\boldsymbol{l}}$, is a weighted function of well logs from different wells denoted by the subscript $\boldsymbol{k}$. If I simplify the prediction to one unknown log and one known log, Equation 3.1 simplifies to the following linear relationship:

$$\boldsymbol{W_k(z)}\tilde{\boldsymbol{l}}\boldsymbol{(z)} \approx \boldsymbol{W_k(z)l_k(S_k(z))}, \tag{3.2}$$

where $\boldsymbol{W_k(z)}$ weights the specific value used to estimate the missing log value, $\tilde{\boldsymbol{l}}\boldsymbol{(z)}$, from an available well logs, $\boldsymbol{l_k(S_k(z))}$. To estimate a missing log at each depth sample, I must remove structural and stratagraphic variations between the well logs by correlating the well logs to common geologic time using function, $\boldsymbol{S_k(z)}$, based on the shifts estimated from LSIM. The correlation is done by selecting a well log type that is available in all wells, for example, gamma ray. We, then, select one reference gamma ray log and estimate the function, $\boldsymbol{S_k(z)}$, that aligns all remaining gamma ray logs to the reference. $\boldsymbol{S_k(z)}$ is applied to the remaining well logs to align all well logs (e.g., density and velocity) to constant geologic time.

I design the weight, $\boldsymbol{W_k(z)}$, in Equation 3.2, as a product of two factors: the distance between the unknown and available well logs and the caliper value at that depth, which measures the size of the borehole at each depth. I make the assumption

that deviations in the caliper from the anticipated borehole size while drilling likely indicates an inaccurate log measurement. Thus, $\boldsymbol{W_k(z)}$ can be expressed as:

$$\boldsymbol{W_k(z) = \phi(|x - x_k|) * C_k(S_k(z)),} \tag{3.3}$$

where $\boldsymbol{\phi(|x - x_k|)}$ is a radial basis function, $\boldsymbol{x_k}$ is the well location, $\boldsymbol{x}$ is the well with a missing log, and $\boldsymbol{C_k}$ is inversely proportional to the deviation between the expected and actual caliper value at each depth.

There are several different radial basis functions, and I chose to implement the inverse multiquadratic radial function

$$\boldsymbol{\phi(|x - x_k|) = \frac{1}{\sqrt{1 + (\epsilon|x - x_k|)^2}}} \quad \text{, where } \boldsymbol{\epsilon > 0} \tag{3.4}$$

which gives a larger weight to a well closer to the unknown well as compared to a well farther away.

Returning to our original linear relationship, Equation 3.1, the estimated log, $\boldsymbol{\tilde{l}}$, is a function of available well logs and weighted by each well's distance and caliper log. By solving the least-squares problem in Equation 3.1, I can predict a new 'pseudo well log' at each depth as follows:

$$\boldsymbol{\tilde{l(z)} = \frac{\sum_{k=1}^{N} W_k^2(z) l_k(S_k(z))}{\sum_{k=1}^{N} W_k^2(z)}} \tag{3.5}$$

I use wells from the Teapot Dome dataset from Wyoming made available by the U.S. Department of Energy and RMOTC to test the proposed approach. Over 1000 wells have been drilled into the anticline structure. I select a limited subset of the 26 longest wells for our examples summarized in Table 3.1. Several wells have

missing sonic or density logs making it challenging to integrate the available log and seismic data. In this section, I focus on using the sonic, density, caliper and gamma ray logs to estimate a complete sonic and density well log suite that are the minimum required logs to estimate a TDR and model a synthetic seismogram to perform a seismic well tie. Table 3.2 summarizes the initial well log dataset that is used in this section.

Table 3.1: Well logs used in examples. Data pulled directly from Teapot Dome dataset made available by the U.S. Department of Energy and RMOTC.

UWI	Sonic	Density	NPHI	Caliper[1]	Caliper[2]	Gamma Ray[1]	Gamma Ray[2]
49025109020000	X				X		X
49025107090000	X	X	X		X		X
49025109200000	X	X	X	X		X	
49025110490000	X	X		X		X	
49025106100000	X	X	X		X		X
49025110120000	X		X		X	X	
49025107450000		X	X		X		X
49025108070000		X	X		X		X
49025110700000	X			X		X	
49025107690000		X	X		X		X
49025107260000		X	X		X		X
49025107290000		X	X		X		X
49025109720000	X	X		X		X	
49025109370000	X	X	X		X	X	
49025102650000		X	X		X		X
49025108310000	X	X	X		X	X	
49025109650000	X	X	X	X		X	
49025109730000	X	X	X		X	X	
49025109660000	X	X	X	X		X	
49025105980000		X	X		X		X
49025109060000	X	X	X	X		X	
49025109710000	X	X		X		X	
49025106090000		X	X		X		X
49025108910000		X	X		X		X
49025108970000		X	X		X		X
49025102700000			X		X		X

Derived from [1]resistivity and [2]density logs

Table 3.2: Well log data statistics for sonic, density, caliper and gamma logs

Log Type	Wells	Sonic	Density	Caliper*	Gamma*
Number	26	15	22	26	26
Mean Length (ft)	4192	2646	3093	4074	4074

*Derived from resistivity and density logs as provided with the dataset made available by RMOTC.

From Equation 2.12, to align all wells to a constant geologic time, I estimate

the warping function, $\boldsymbol{S_k(z)}$. Because a form of a gamma ray log are available in all wells, I use the gamma logs to estimate the warping function. The longest gamma ray log is selected as the reference log, $\boldsymbol{r(z)}$. The shifts are estimated by matching the gamma ray log from each well to the reference gamma log as shown in Figure 3.2(a). The alignment shifts are then applied to the remaining well logs at each well to align all well logs to constant geologic time. Results of aligning a sonic log before and after applying the shifts estimated from aligning the gamma ray logs are shown in Figures 3.1(b) and 3.2(b), respectively.

This approach results in a well log dataset flattened along constant geologic time. The log data might be collected over several years, with different logging tools, and likely different techniques applied to process the data. To account for this variability, I normalize the sonic and density logs using the big histogram method (Shier et al., 2004). For normalization, I select 15 intervals based on available well log tops and lithology variations. I estimate the cumulative mean and standard deviation for all well log data in each interval. I assume that the distribution of well log data from each well, in each interval, should fall one standard deviation of the cumulative mean. Normalization in the constant geologic time domain requires little interpreter input as each log is inherently stratigraphically correlated. With the aligned and normalized sonic logs, I estimate the missing sonic logs, or sections of sonic logs using Equation 3.5.

I perform a blind well test to validate the proposed approach by estimating a sonic log in a well where a real sonic log is available; the estimated sonic log is crossplotted against the real sonic log for the entire well in Figure 3.3(b). For comparison purposes, I use available density information and the Reverse Gardner Equation (Gardner et al., 1974) to estimate a sonic log; this result is crossplotted

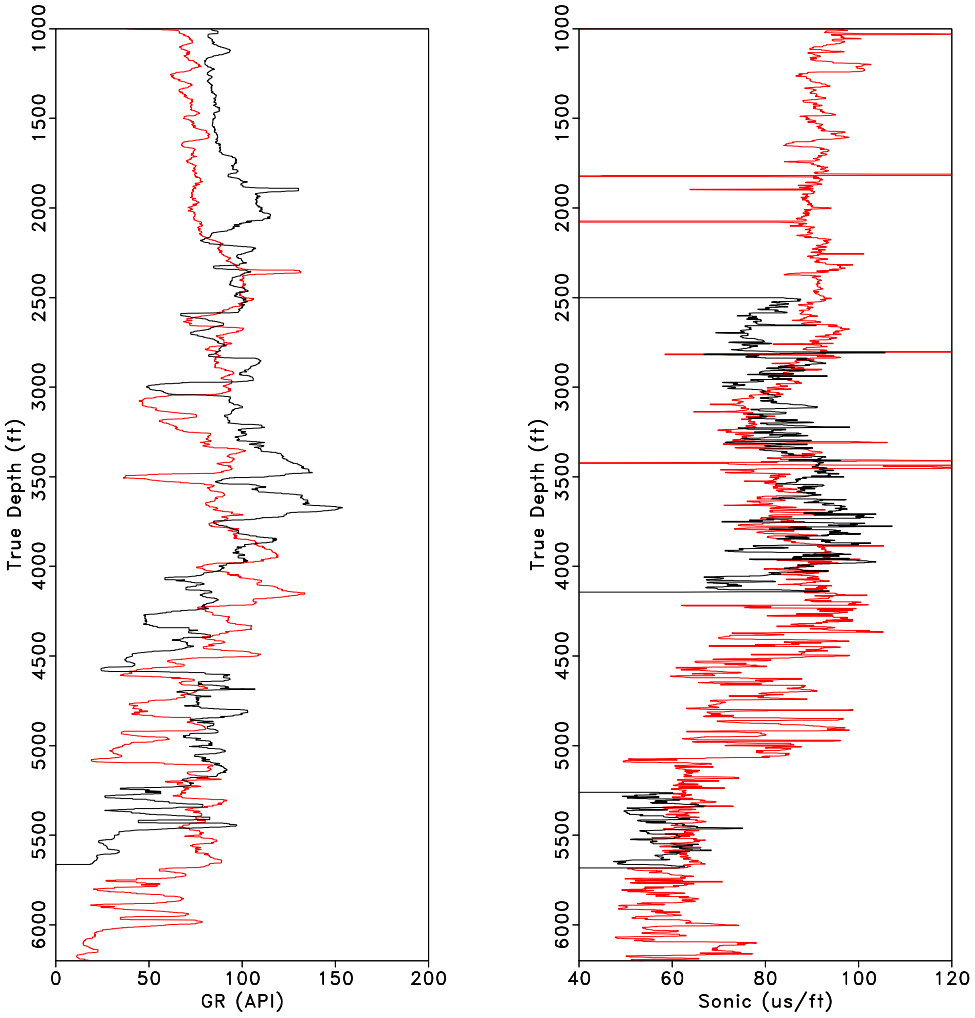

(a) (b)

Figure 3.1: (a) Median filtered gamma log from the reference well (red) and median filtered gamma log from a second well (black). (b) Sonic log from the reference well (red) and sonic log from a second well (black). ch03-logs/../interpPaper/logs GR0and2,DT0and2

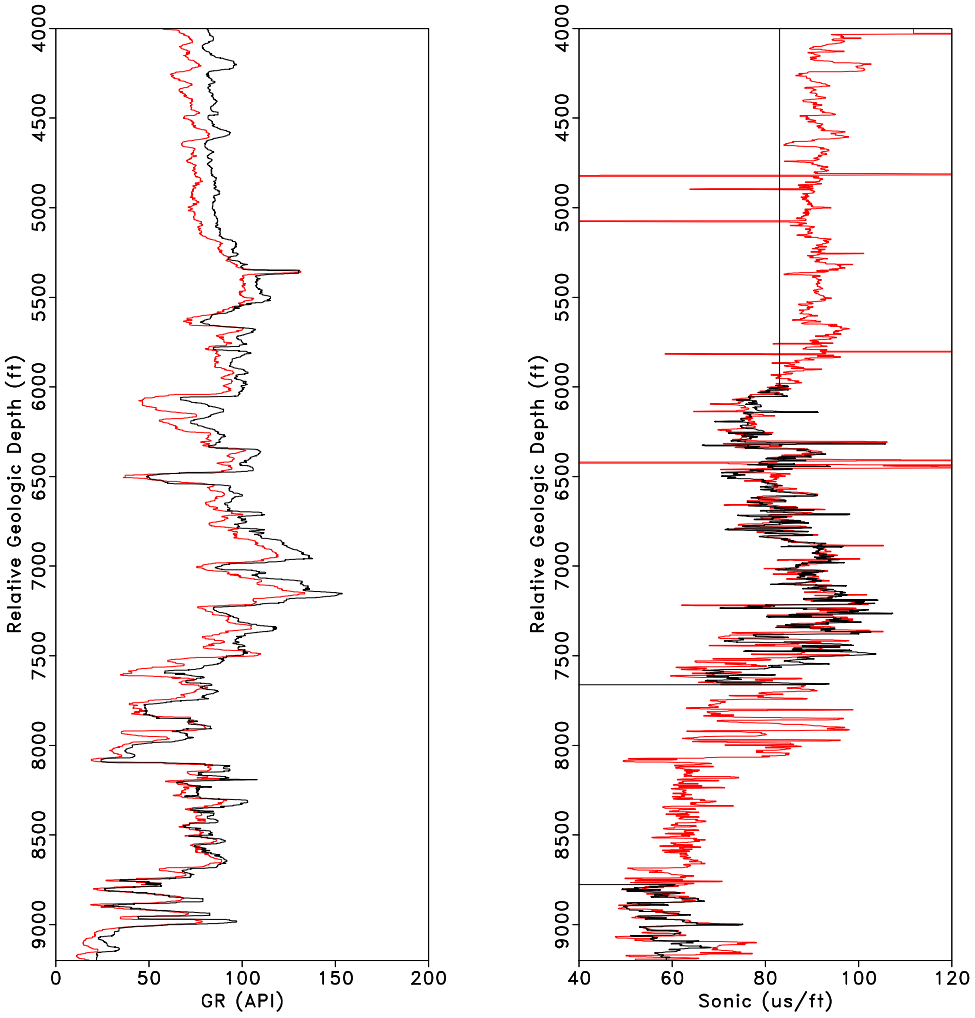

(a) (b)

Figure 3.2: (a) Median filtered gamma log from the reference well (red) and an aligned gamma log from a second well (black) after applying estimated alignment shifts. (b) Sonic log from the reference well (red) and an aligned sonic log from a second well (black) after applying estimated alignment shifts from matching gamma logs. ch03-logs/../interpPaper/logs GR2shift0,DT2shift0

against the real sonic log for the entire well in Figure 3.3(a). When estimating the Reverse Gardner Equation, I break the well into 15 intervals based on well tops and changes in lithology from the gamma ray log, and I recompute the equation that best fits the data for each interval. I observe significant improvement of the proposed approach over a conventional method for estimating a missing sonic log. Results comparing the sonic log estimated using the proposed approach against the real sonic log along two 1600 ft intervals are shown in Figure 3.4.

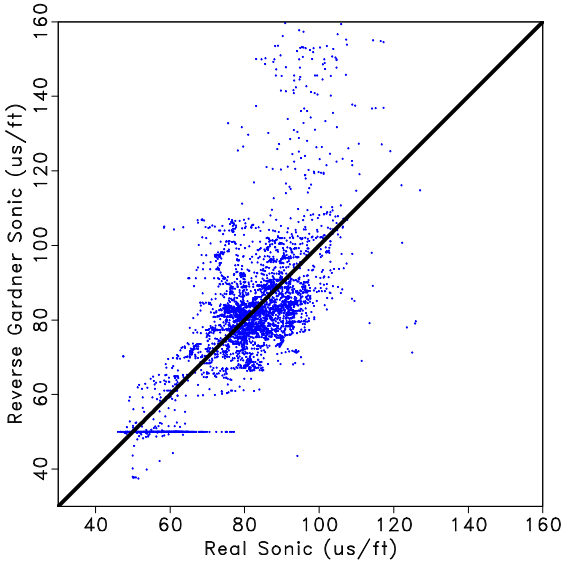

(a)

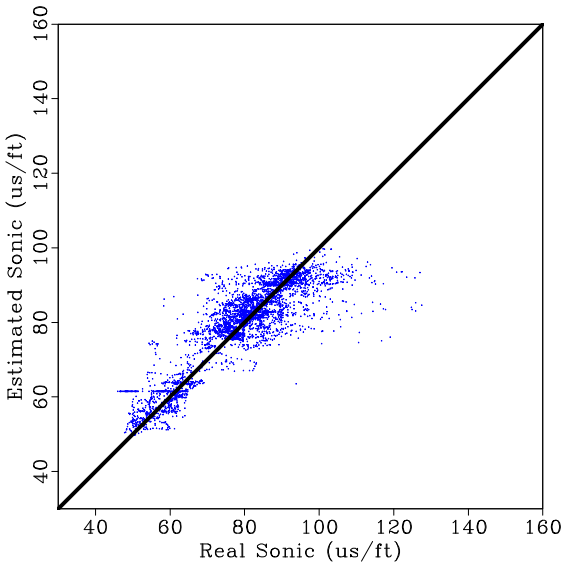

(b)

Figure 3.3: (a) Real sonic log cross plotted against the sonic log estimated using Reverse Gardner equation. (b) Real sonic log cross plotted against the sonic log estimated using the proposed approach. ch03-logs/../interpPaper/logs xplot-DT2gard,xplot-DT2

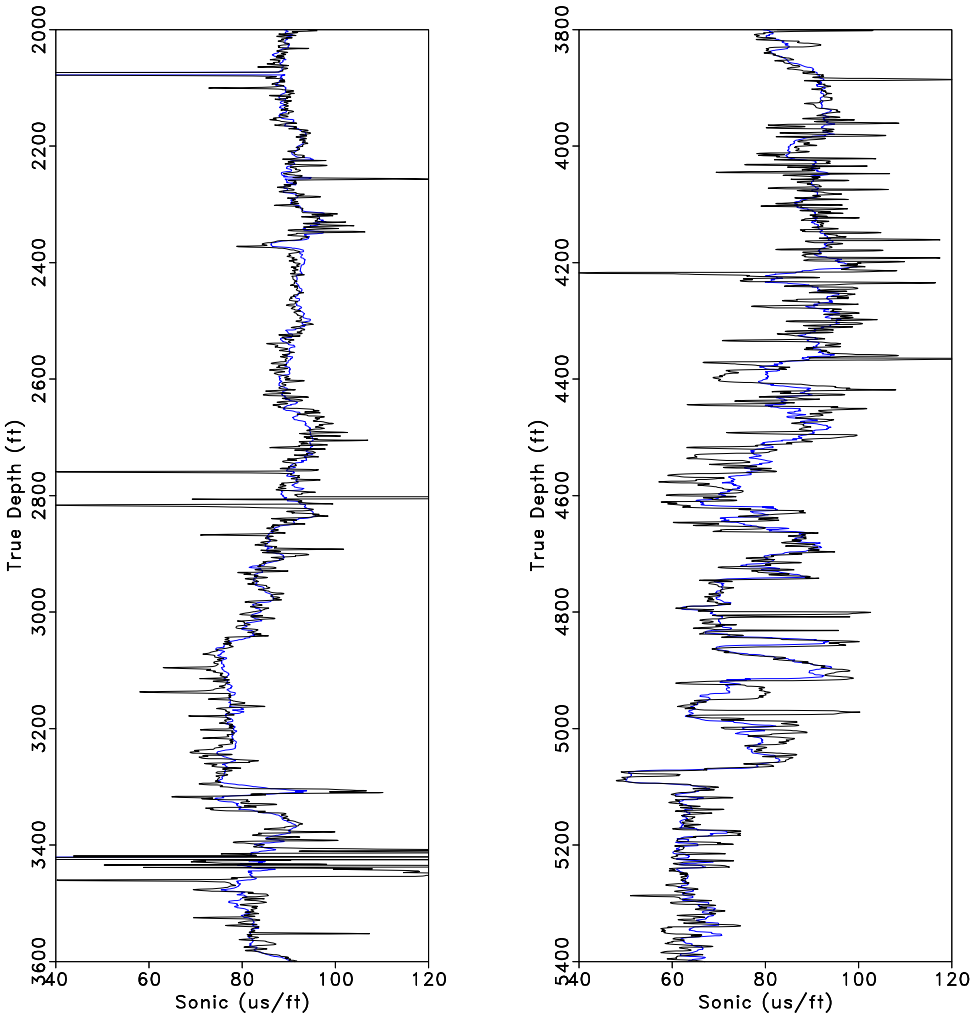

(a) (b)

Figure 3.4: I perform a blind well test by estimating a sonic log using the proposed approach and comparing the result against the real sonic log. Real sonic log (black) versus estimated sonic log (blue) along two 1600ft intervals along the reference log. ch03-logs/../interpPaper/logs DT01p0,DT02p0

From Equation 3.4, there are two user selected constants: $\boldsymbol{\epsilon}$ in the RBF and the weighting of the caliper, $\boldsymbol{C_k}$. To select optimal values for these constants, I minimize the average RMS error of every predicted sonic and density log against the actual sonic and density logs.

$$\boldsymbol{RMS_{error}} = \frac{\sum_{k=1}^{N} \sum_{z=0}^{z_{max}} \sqrt{(\tilde{l_k}(S_k(z)) - l_k(S_k(z))^2}}{N} \tag{3.6}$$

where $\tilde{\boldsymbol{l_k}}$ is the blind well test prediction of log $\boldsymbol{k}$ and $\boldsymbol{l_k}$ is the actual log $\boldsymbol{k}$. This minimization problem is visualized in Figure 3.5 where Equation 3.6 is solved for different values of $\boldsymbol{\epsilon}$ in Equation 3.4 when estimating a sonic and density log.

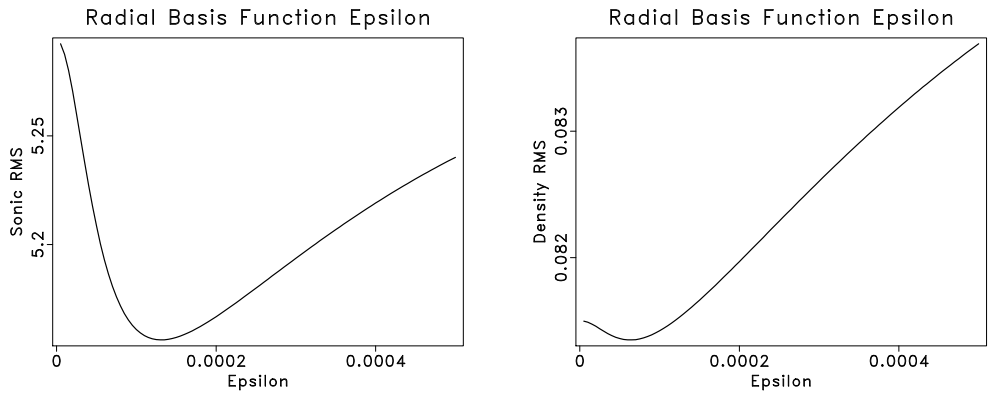

(a) (b)

Figure 3.5: (a) RMS error between real and predicted sonic logs given all wells in the dataset and $\boldsymbol{\epsilon}$ values. (b) RMS error between real and predicted density logs given all wells in the dataset and $\boldsymbol{\epsilon}$ values. ch03-logs/sens epsdt,epsrhob

I normalize and combine the results shown in Figures 3.5 to select a single value of $\boldsymbol{\epsilon}$ that minimizes Equation 3.6 for sonic velocity and density. The constant controlling the weighting of the caliper, $\boldsymbol{C_k}$, is also estimated by combining the normalized result of Equation 3.6 for different caliper weighting values. Results of this

combination are shown in Figure 3.6, where I observe minimum normalized RMS error when $\boldsymbol{\epsilon = 0.0001}$ and $\mathbf{weight_{caliper} = 0.423}$.

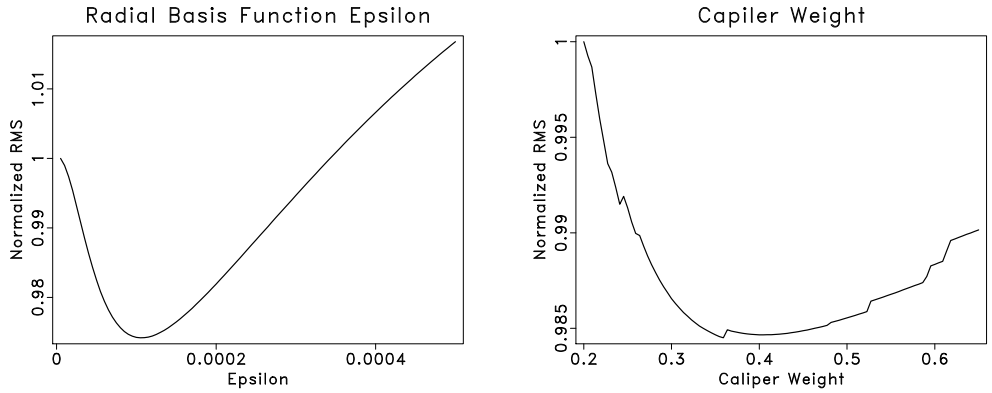

(a) (b)

Figure 3.6: (a) Normalized combined sonic and density RMS error given all wells in the dataset and $\boldsymbol{\epsilon}$ values. (b) Normalized combined sonic and density RMS error given all wells in the dataset and caliper weighting values. ch03-logs/sens eps,cal

From Table 3.2, I observe that most wells have a sonic and density log; however, the difference between the mean length of the sonic/density logs as compared to the gamma log indicates that several of the well logs were not acquired over specific intervals or have missing sections as shown in Figure 3.2(b). For well logs that have missing sections, I include the available log data in Equation 3.5 to honor the available measurements and interpolate the missing log sections. In Figure 3.7 we interpolate missing log data where there are holes in the original log and make use true well log measurements when available.

The proposed approach is applied to 26 wells from the Teapot Dome dataset to generate complete sonic and density logs for each well. Table 3.3 summarizes the log dataset after estimating missing or incomplete logs.

By estimating missing sonic and density logs for each well, I increase the

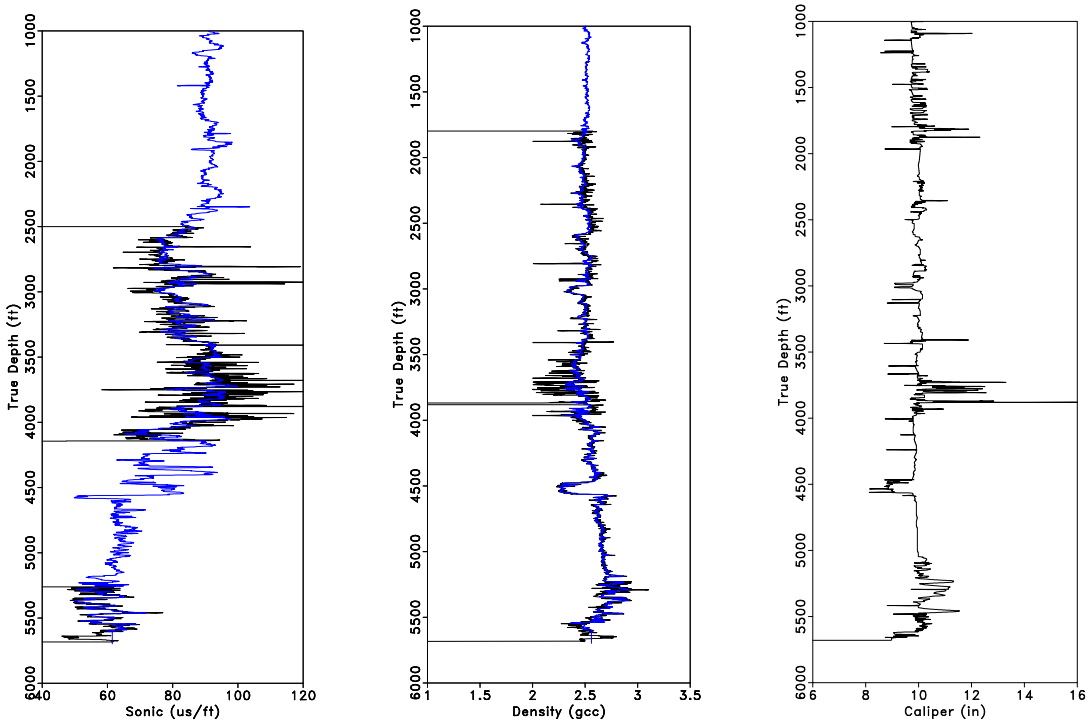

(a) (b) (c)

Figure 3.7: (a) Original sonic log (black) versus estimated sonic log (blue). (b) Original density log (black) versus estimated density log (blue). The original well log data is used in the inversion so areas where sonic or density data is available the estimated logs match the original data. In the interval between 3500 ft and 3900 ft, there is a significant deviation in the (c) caliper log indicating an inaccurate measurement; therefore, the estimated log deviates significantly from the original log.
ch03-logs/../interpPaper/logs DTp2a,RHOBp2a,CAL2

Table 3.3: Well log data statistics after estimating sonic and density logs for all wells

Log Type	Wells	Sonic	Density	Caliper*	Gamma*
Number	26	26	26	26	26
Mean Length (ft)	4192	3991	3639	4074	4074

*Derived from resistivity and density logs as provided with the dataset made available by RMOTC.

number of logs and length of the logs available to integrate with the available seismic data. Using the interpolated sonic and density logs, it is possible to compute a TDR and reflectivity series to tie any given well to seismic data. The proposed method addresses several challenges in integrated studies, specifically interpolating missing well logs at wells that have incomplete well log suites and may be a useful data integration tool in onshore plays where the number of wells drilled is much higher compared to the number of sonic and density log acquired.

Although this method addresses several challenges, I focus on interpolation techniques that assume that rock-properties do not vary significantly laterally and make several additional assumptions related to the interpolation of missing log data:

1. Gamma logs are matched to estimate the alignment shifts; therefore, estimated section is limited to a section in each well with an available gamma log.

2. All gamma logs are aligned with a single reference gamma log and the estimated log section is limited to the stratigraphy found in this reference log. This reference well log can be thought of as a type log which contains the entire stratigraphic column observed in other well logs.

3. I did not perform fluid substitution prior to solving equation 3.5 for each well. The proposed approach is based on interpolation, and I assume fluid substitution to have a negligible impact on the results. This assumption may present

challenges in reservoirs where hydrocarbons impact the well response within the same stratigraphic interval.

These assumptions may not be valid in geologically complex areas with significant stratigraphic variations such as unconformities or channels where entire stratigraphic units may be absent due to erosion. Additionally, the well log correlation approach, may meet similar challenges as those experienced by conventional, interpreter driven, workflows where rapid stratigraphic variability (e.g. slope deposits, clinoforms, etc.) may not correlate, or may correlate ambiguously in several places, between wells. Although I did not account for changes in the fluid content, the proposed approach provides a reasonable first-order approximation of the unknown well logs. The predicted velocity and density well logs provides the minimum required logs to forward model a synthetic seismogram and tie the well with real seismic data, which is discussed in the next chapter.

Missing well log data prediction using Bayes' theorem*

The previously proposed method for missing log data prediction is useful; however, the method is based on interpolation and does not consider information at the same well location. Additionally, well log data do not perfectly conform to empirical estimations (see Figure 2.5); there is often scatter of the real data around the empirical models. Methods that consider all well log data and the uncertainty of these measurements relative to empirical estimations and models might provide the best approach to estimating missing log data. Avseth et al. (2010) show that probabilistically modeling reflectivity from distributions of $\boldsymbol{V_p}$, $\boldsymbol{V_s}$, and $\boldsymbol{\rho}$ and comparing modeled

*Parts of this section are published in Bader et al. (2018b).

gradient-intercept against inverted gradient-intercept data from seismic amplitudes results in a facies distribution consistent with observations from wells. I theorize that using a distribution around a model will improve on the previously proposed method of missing well log prediction.

I propose a method to estimate missing sonic logs in the relative geologic time domain using sonic logs acquired at other wells as well as non-sonic well logs at the well with the missing sonic log. I first correlate a reference gamma log from each well using LSIM and employ the estimated shifts to align all available logs. In the relative geologic time (RGT) domain, I interpolate a missing sonic log according to the previously proposed approach, using sonic logs acquired at other wells; this result is treated as a priori information. I then use the stratigraphically correlated sonic, density and neutron porosity logs to perturb the a piori information using Bayes' theorem. The maximum a posteriori estimate is compared against the actual sonic log using a blind well test. Results of this method show an improvement over previously proposed methods that use only one of the three available sources of information to predict a missing well log.

I perturb the interpolated sonic log from Equation 3.5 based on available density and neutron porosity logs acquired at the well of interest. If I treat the interpolated sonic result as prior information, $\boldsymbol{p(m)}$, I use Bayes' theorem to estimate a posterior result given a likelihood function based on porosity and density logs acquired at the well of interest, $\boldsymbol{l(d|m)}$, as follows:

$$\boldsymbol{\sigma(m|d) \propto l(d|m)p(m)} \tag{3.7}$$

The likelihood function incorporates correlated modeled distributions between

sonic, density and porosity based on the well log data in each stratigraphic interval. The trends for the correlated distributions are from empirical relationships: Gardner's relationship, which relates sonic and density log data for a large number of brine saturated rocks, and the general relationship between bulk density and porosity (Gardner et al., 1974). I start with Gardner's relationship to relate density to velocity,

$$\boldsymbol{\rho_b = \alpha v_p^{\beta}.} \tag{3.8}$$

where

$\boldsymbol{v_p}$ = P-wave velocity in $\mathbf{ft/s}$

$\boldsymbol{\rho_b}$ = Bulk density from log in $\mathbf{g/cm^3}$

$\boldsymbol{\alpha}$ = Constant, estimated for each stratigraphic interval

$\boldsymbol{\beta}$ = Constant, estimated for each stratigraphic interval

I combine Gardner's relationship with the general relationship between bulk density and porosity,

$$\boldsymbol{\phi_T = \frac{\rho_m - \rho_b}{\rho_m - \rho_f},} \tag{3.9}$$

where

$\boldsymbol{\rho_m}$ = Matrix density in $\mathbf{g/cm^3}$

$\boldsymbol{\rho_f}$ = Fluid density in $\mathbf{g/cm^3}$

to obtain a relationship between p-wave velocity and total porosity,

$$\boldsymbol{\phi_T = \frac{\rho_m - \alpha v_p^{\beta}}{\rho_m - \rho_f}.} \tag{3.10}$$

To estimate total porosity, $\boldsymbol{\phi_T}$, I combine density porosity and neutron porosity as follows:

$$\boldsymbol{\phi_T \approx \sqrt{\frac{(\phi_D)^2 + (\phi_N)^2}{2}}}, \tag{3.11}$$

where $\boldsymbol{\phi_D}$ and $\boldsymbol{\phi_N}$ are the density porosity and the neutron porosity in sandstone units, respectively, from well logs. Density porosity is calculated from the density log using Equation 3.9 assuming a matrix density of sandstone and fluid density of fresh water.

I combine Equations 3.8, 3.9, and 3.10 with the distributions of sonic, density and total porosity to generate a multivariate probability distribution function for each stratigraphic interval. I solve Equation 3.7 for the maximum a posteriori estimate given the a priori interpolated sonic log, the density log and total porosity log (from logs acquired at the well).

To test the proposed approach, I use the wells and associated well log summarized in Table 3.1. The values for $\boldsymbol{\alpha}$, $\boldsymbol{\beta}$, $\boldsymbol{\rho_m}$, and $\boldsymbol{\rho_f}$ in Equations 3.8, 3.9, and 3.10 are estimated independently for each stratigraphic interval.

The prior distribution is modeled using the interpolated sonic well log, and the true density and total porosity logs acquired at the well location. I consider the interpolated sonic log to have significant uncertainty as compared to the density and total porosity measurements, which are acquired at the well. The bivariate prior distributions for one depth are shown in Figures 3.9(a), 3.9(b), and 3.9(c).

The likelihood distribution is modeled from the empirical relationships and the distributions of the initial, normalized, well log data in each stratigraphic interval.

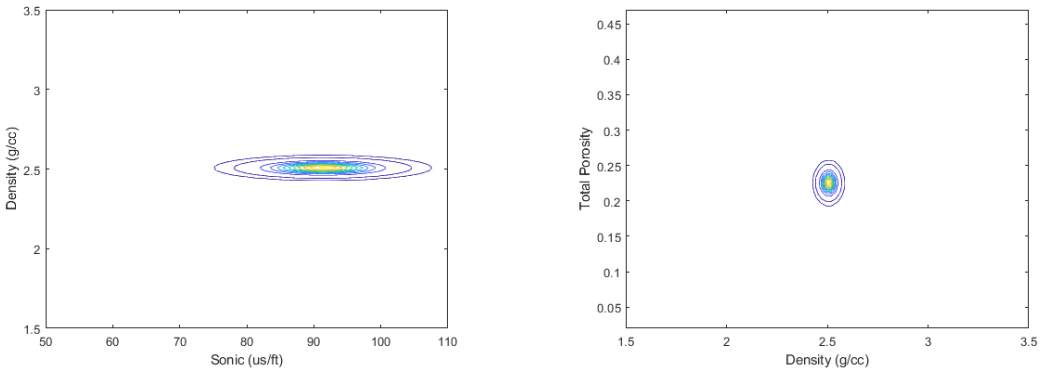

(a)

(b)

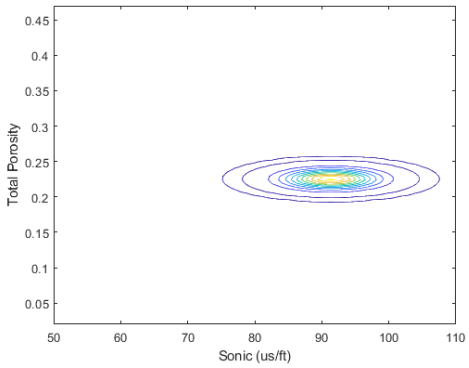

(c)

Figure 3.8: (a) Sonic and density bivariate prior distribution at one depth. (b) Density and total porosity bivariate prior distribution at one depth. (c) Sonic and total porosity bivariate prior distribution at one depth. The sonic log value is interpolated using the method described previously and has higher uncertainty as compared to well logs acquired at the well. ch03-logs/../logbayes/exp logbays-sonic-rhob-p,logbays-rhob-poro-p,logbays-sonic-poro-p

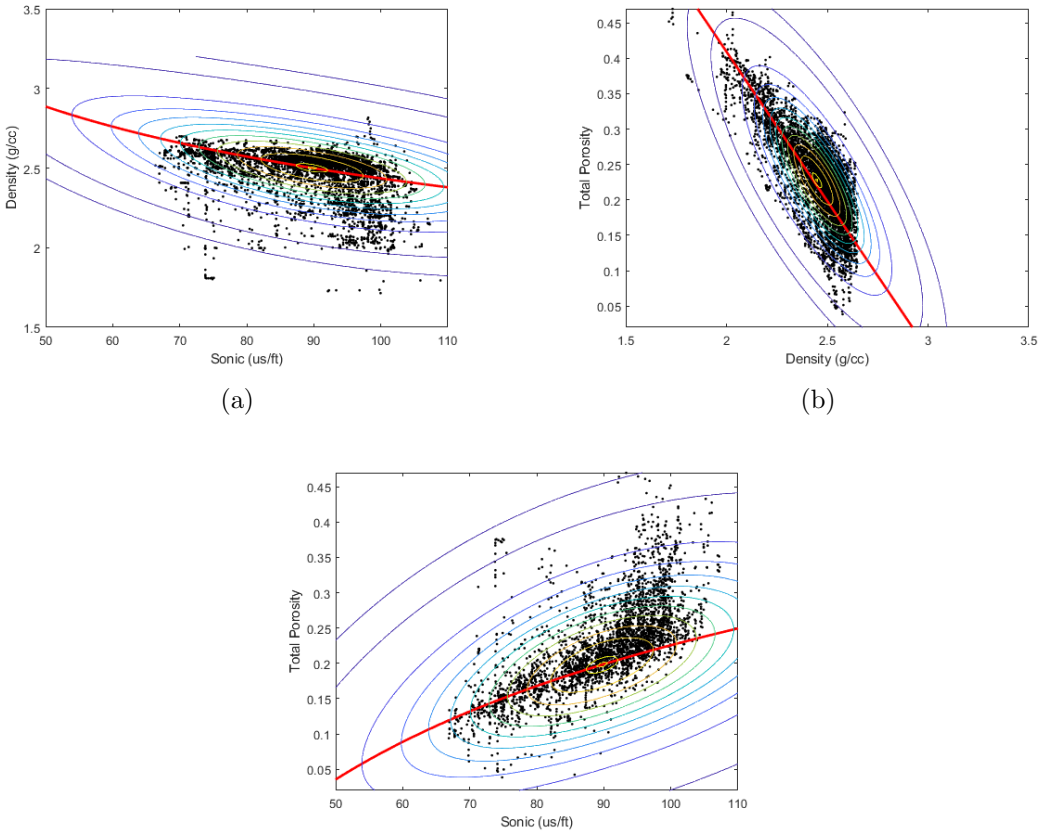

Figure 3.9: (a) Bivariate likelihood distribution (contours) for sonic and density well log data in one stratigraphic interval. (b) Bivariate likelihood distribution (contours) for density and total porosity well log data in one stratigraphic interval. (c) Bivariate likelihood distribution (contours) for sonic and total porosity well log data in one stratigraphic interval. Actual well log data (black dots) in one stratigraphic interval. The red line is an empirical estimation Equations 3.8, 3.9, and 3.10.
ch03-logs/../logbayes/exp logbays-sonic-rhob,logbays-rhob-poro,logbays-sonic-poro

The resulting bivariate likelihood distributions for one interval are plotted with the available well log data and empirical estimations in Figures 3.9(a), 3.9(b), and 3.9(c). I observe that the empirical estimation for each bivariate distribution captures the general trend of the well log data; however, the complete dataset is better represented by including the distribution of the data in our model.

The prior and likelihood functions are used to estimate a posterior distribution in each stratigraphic interval for every depth using Equation 3.7. The maximum a posteriori estimate is selected as the well log velocity value at a given depth. I compare the prior sonic log to the real sonic log (Figure 3.10(a)) and the posterior sonic log to the real sonic log (Figure 3.10(b)). At samples where the real sonic log is available, we cross plot the prior versus real sonic log (Figure 3.11(a)) and the posterior versus real sonic log (Figure 3.11(b)). The correlation between the prior and real sonic log is **85.76%** and the correlation between the posterior and real sonic log is increased **89.43%**.

The proposed approach uses Bayes' theorem to combine uncertainty with empirical equations to estimate a missing sonic log using several available datasets. My experiments demonstrate that combining several well log types and empirical estimations provide an improvement* over our a-priori sonic log based on the previously proposed interpolation method**.

*Results are further verified by comparing a modeled synthetic seismogram against real seismic data; these results are presented in the Appendix.

**Although the missing well log data prediction using Bayes' theorem provides the well log most consistent with all available well log data, in this thesis I use Equation 3.5 to predict missing sonic and density well logs for estimating a reflectivity series and TDR.

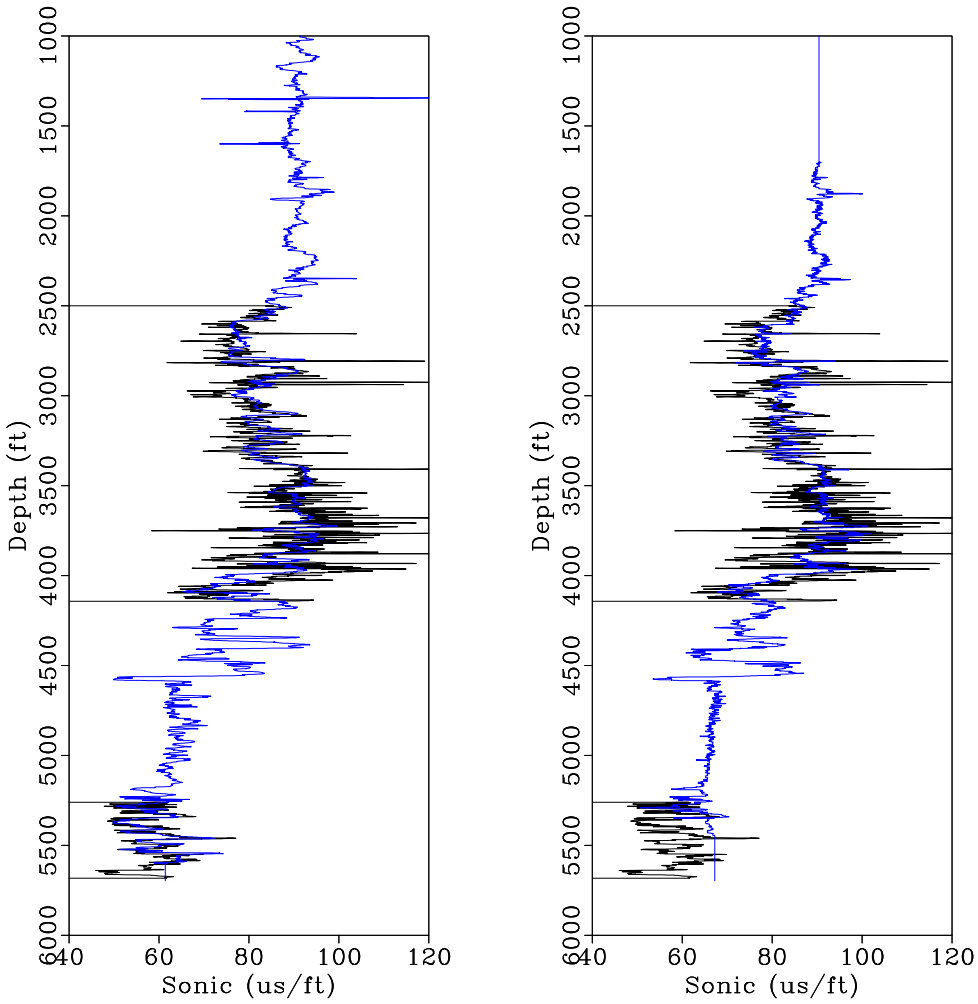

(a) (b)

Figure 3.10: (a) A priori sonic log (blue) estimated from available sonic logs in the dataset and (b) posterior sonic log estimated using the proposed approach (blue). Each estimated sonic log is compared against the real sonic log (black). ch03-logs/../logbayes/exp DT2priorF,DT2bayesF

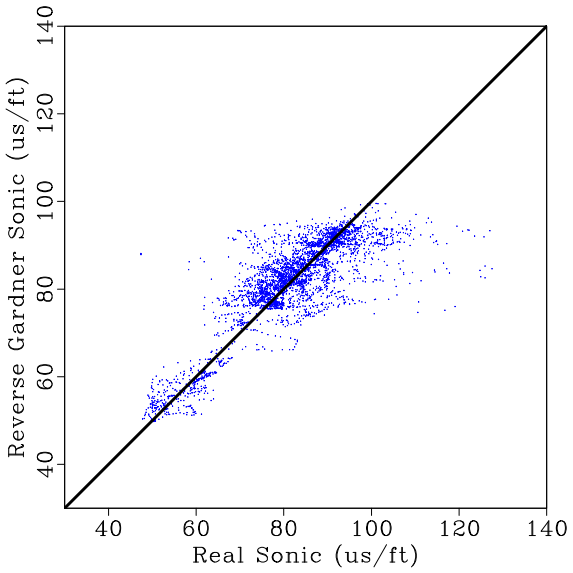

(a)

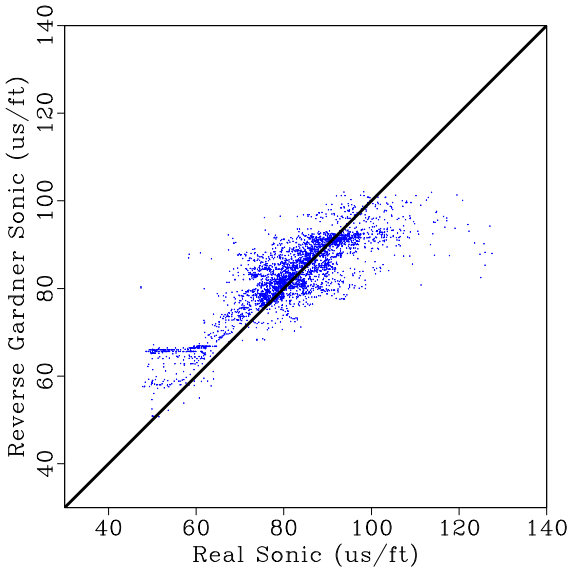

(b)

Figure 3.11: (a) Real sonic log cross plotted against the a priori sonic log. (b) Real sonic log cross plotted against the maximum a posteriori sonic log estimated using the proposed approach. There is a subtle improvement using the proposed approach ch03-logs/../logbayes/exp xplot-DT2prior,xplot-DT2bayes

Chapter 4

Seismic-Well Ties

While the log data provides one source of information to understand the subsurface, an additional source of information is the 3D seismic dataset. Seismic-well ties can be used to understand amplitude variations in seismic data, which has vertically lower resolution but higher spatial coverage, whereas the well logs can provide vertically higher resolution but are measured only at limited locations. This calibration involves generating a reflectivity series from available logs, estimating a wavelet from seismic data, and matching common reflectors between the modeled synthetic and seismic data. The latter step tends to be the most time consuming and subjective process, as manual matching of reflectors usually involves stretching and squeezing of the synthetic until a desired of correlation between the data sets is achieved (White and Simm, 2003). To address the challenge of consistency and accuracy of seismic well ties, I propose to use LSIM to automatically tie the modeled synthetic to seismic data.

Seismic-well ties using LSIM scan and velocity update*

Returning to my first example of a seismic-well tie, in Figure 2.3, I observe a reasonable alignment between the modeled synthetic seismogram and the seismic

*Parts of this section are published in Bader et al. (2018c).

data with only a bulk shift - likely related to missing a shallow section of the velocity log (Bianco, 2014). I extract the closest trace to the well location and compare it with the modeled synthetic from the well log data in Figure 4.1. When compared, I observe a mis-tie between the modeled synthetic and seismic trace between 1.5 and 2.6 seconds. This mis-tie can be related to a number of problems including incorrect migration velocity, anisotropy, attenuation and dispersion (White and Simm, 2003). In Chapter 6, I will further discuss on the relationship between a seismic mis-tie, the migration velocity model and anisotropy.

I use LSIM to estimate the shifts to align the synthetic seismogram with the real seismic trace. The LSIM scan is shown in Figure 4.2, whereas the warm colors indicate high similarity (high correlation) between the synthetic seismogram and real seismic trace while the cold colors indicate low similarity (high correlation) between the synthetic seismogram and real seismic trace. The trend selected in Figure 4.2 maximizes the correlation between the synthetic seismogram and real seismic trace. This trend is applied to the original synthetic seismogram to align with the seismic trace in Figure 4.3.

After applying the shifts, I observe reasonable alignment between the modeled synthetic seimogram and the real seismic trace along the entire length of both datasets. Prior to applying the alignment shifts, the correlation coefficient between the synthetic and real traces in the window of 1 to 2.7 seconds is $\mathbf{-0.333602}$. After applying the alignment shifts, the correlation coefficient between the synthetic and real traces in the window of 1 to 2.7 seconds is $\mathbf{0.77642}$. Additionally, I use LSIM to compute the shifts required to align the synthetic seismogram with the seismic trace a second time in Figure 4.4 and observe little to no relative shifts required to further align the synthetic to the seismic trace.

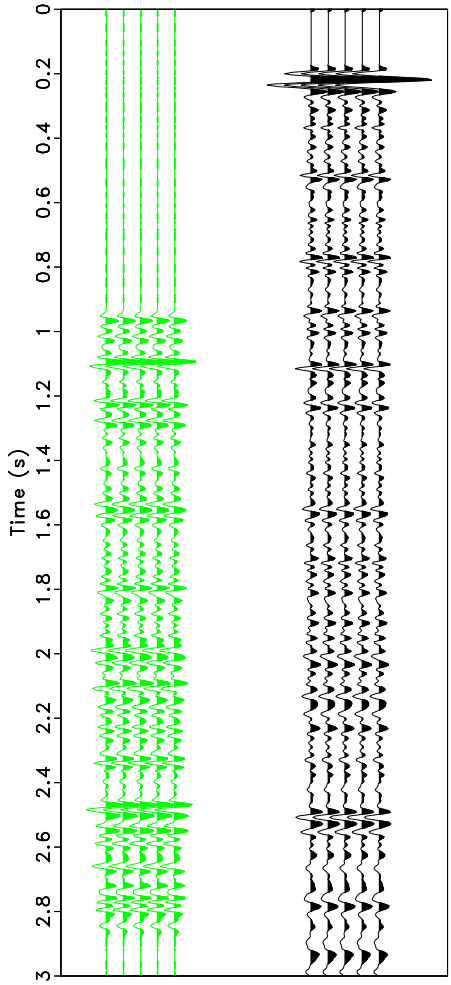

Figure 4.1: Synthetic modeled using the initial sonic log (green). Closest trace to the well location extracted from the phase adjusted seismic data (black). ch04-welltie/../ch02-review/smpltie synth-s0

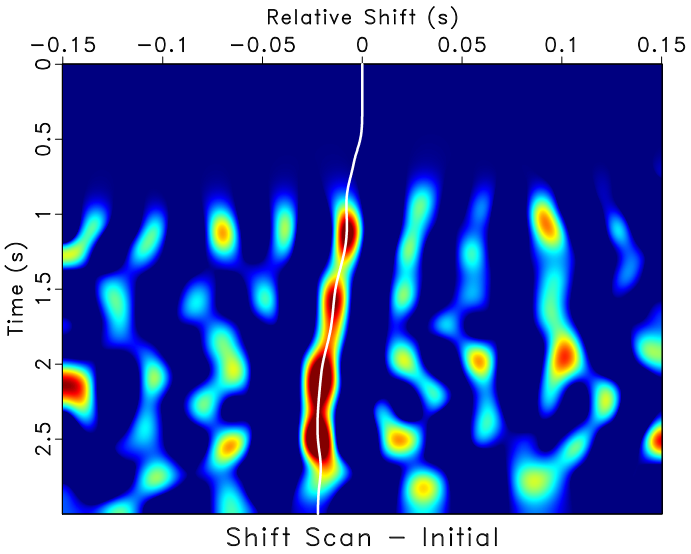

Figure 4.2: Similarity scan between the modeled synthetic seismogram and the real seismic trace. The warm colors indicate high similarity (high correlation) between the synthetic seismogram and real seismic trace whereas the cold colors indicate low similarity (high correlation) between the synthetic seismogram and real seismic trace.
ch04-welltie/../ch02-review/smpltie scan

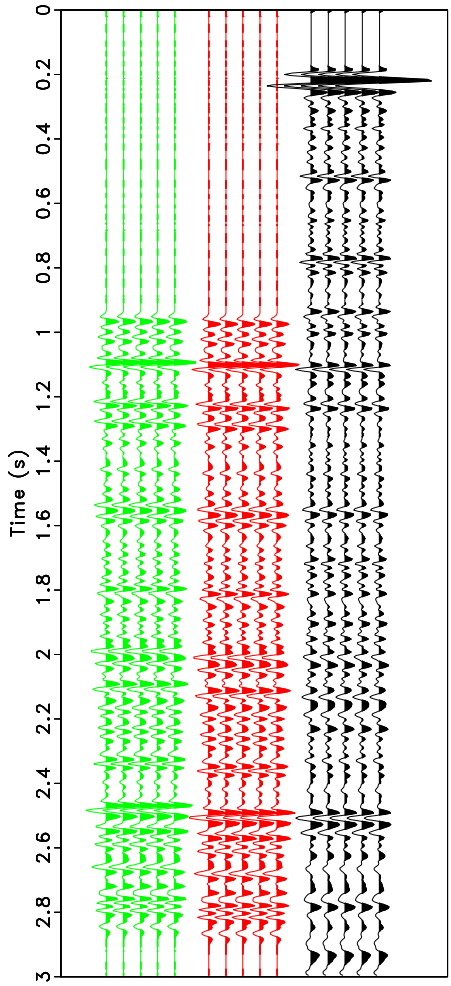

Figure 4.3: Synthetic modeled using the initial sonic log (green). Synthetic modeled using the sonic log updated after one iterations of matching using LSIM to estimate shifts (red). Closest trace to the well location extracted from the phase adjusted seismic data (black). ch04-welltie/../ch02-review/smpltie synth-s1

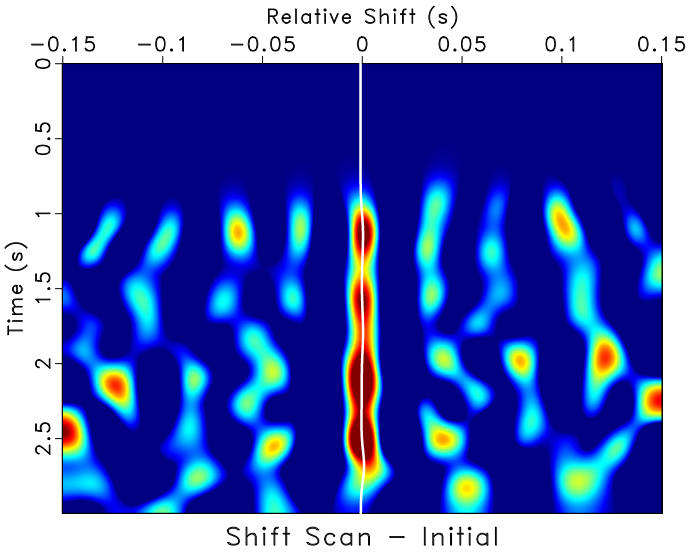

Figure 4.4: Similarity scan between the modeled synthetic seismogram and the real seismic trace. The warm colors indicate high similarity (high correlation) between the synthetic seismogram and real seismic trace while the cold colors indicate low similarity (high correlation) between the synthetic seismogram and real seismic trace. Notice high similarity values aligned along zero relative shift indicating no shifts are required to align the synthetic seismogram with the seismic trace. ch04-welltie/../ch02-review/smpltie scanch4

By applying the shifts to align the synthetic seismogram with the seismic trace, I am ensuring consistency between well log and seismic data; however, this alignment manifests itself as an alteration to the well log velocity. In the time domain, the shifts, $\boldsymbol{g_{k,i}(t)}$ at well $\boldsymbol{k}$, are estimated using several iterations, $\boldsymbol{i}$, of LSIM data matching. Each iteration estimates a smooth sequence of shifts to align the synthetic seismogram with the seismic trace. Muñoz and Hale (2015) and Herrera et al. (2014) observe a relationship between the shifts used to align a synthetic with seismic trace and an updated velocity function:

From Equation 2.13, assuming an initial TDR, $\boldsymbol{T_0}$, I arrive at

$$\boldsymbol{S_{k,1}(T_0) = T_0 + g_{k,1}(T_0)} \tag{4.1}$$

after one iteration of LSIM. I estimate an updated TDR by interpolating our shifts from time to depth

$$\boldsymbol{T_1(z) = T_0(z) + g_{k,1}(T_0(z)).} \tag{4.2}$$

Using Equation 2.4, I relate the initial and updated velocity log to the initial and updated TDR,

$$\boldsymbol{\frac{dT_1(z)}{dz}(\frac{dT_0(z)}{dz})^{-1} = \frac{v_0(z)}{v_1(z)}} \tag{4.3}$$

to solve for the updated velocity log,

$$\boldsymbol{v_1(z) = v_0(z)\frac{dT_0(z)}{dz}(\frac{dT_1(z)}{dz})^{-1}.} \tag{4.4}$$

In my implementation, I use Equation 4.4 to update the velocity function after each iteration. Alternatively, I can directly relate the updated velocity log to the initial velocity log and the estimated shifts. Starting with the derivative of Equation 4.2,

$$\boldsymbol{\frac{dT_1(z)}{dz} = (1 + \frac{g_{k,1}(T_0(z))}{dT_0})\frac{dT_0(z)}{dz},} \tag{4.5}$$

I substitute Equation 4.4 and solve for the update velocity log as follows,

$$\boldsymbol{v_1(z) = v_0(z)\left(\frac{dg_{k,1}(T_0(z))}{dT_0} + 1\right)^{-1}}. \tag{4.6}$$

I use Equation 4.4 to update the velocity log based on the shifts estimated in Figure 4.2. The results of this update are shown in Figure 4.5; I observe a small difference between the original and updated velocity log due to the smooth sequence of shifts estimated using LSIM. The smooth sequence is of shifts is due to the regularization in LSIM. The regularization is reduced significantly in Figure 4.6 to understand how smoothing impacts the sequence of shifts estimated and the velocity well log update.

Qualitatively, I observe more local, high similarity, matches; however the pick is more oscillatory as compared to Figure 4.2. Quantitatively, the correlation coefficient between the synthetic and real traces in the window of 1 to 2.7 seconds is **0.807943**, which greater as compared to the LSIM match using significant regularization in Figure 4.2. The velocity update is related to the shifts by a derivative, so I expect the updated velocity log to be highly oscillatory. The velocity update shown in Figure 4.7 deviates significantly from the original velocity log at 1500ft and below 3700ft by more than 20%. Muñoz and Hale (2015) argue that these significant deviations introduced by the velocity update from the shifts are not reasonable and propose to constrain the shift selection from DTW such that the update can be no greater than $\pm$10%. Although constraining the match in this way may provide a useful result, I argue that this hard constraint may be challenging to parameterize due to the scientific community's general lack of understanding of well tie mis-ties. Alternatively, I implement a soft weighting constraint discussed by White and Simm (2003) based on the energy of the synthetic seismogram as compared against the real seismic trace.

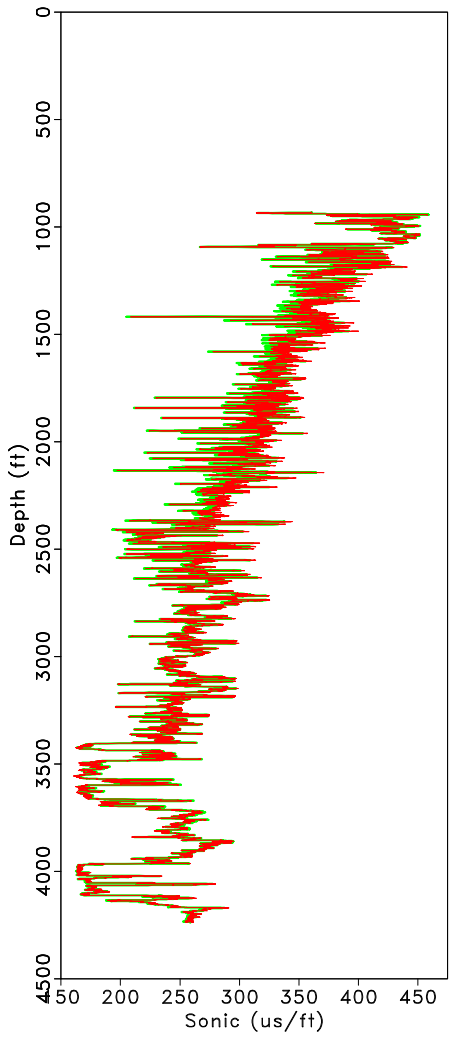

Figure 4.5: Initial sonic log (green). Updated sonic log using the shifts estimated from LSIM to align the synthetic seismogram and real seismic trace (red). ch04-welltie/../ch02-review/smpltie DT-despike-s1

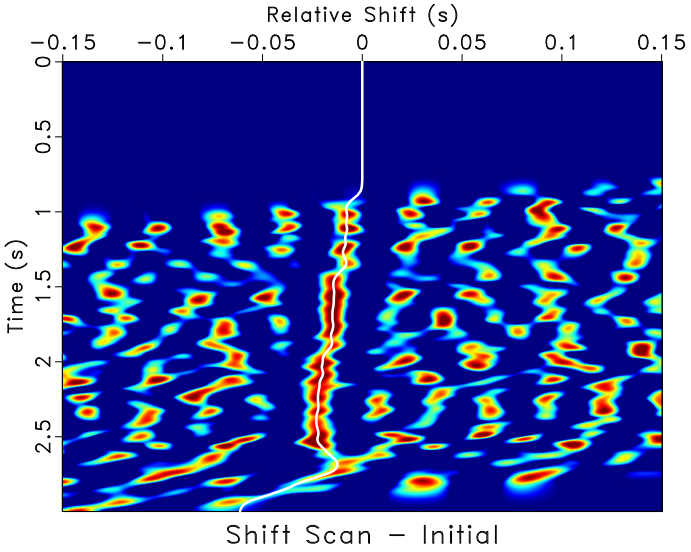

Figure 4.6: Similarity scan between the modeled synthetic seismogram and the real seismic trace. Smoothing is reduced by 80% as compared to Figure 4.2. Notice the oscillatory behavior in the pick from the similarity scan. ch04-welltie/../ch02-review/smpltie scanb

$$\boldsymbol{E(t)} = \sum_{\boldsymbol{k=(t-\frac{R}{2})}}^{\boldsymbol{(t+\frac{R}{2})}} \boldsymbol{A(t)^2} \tag{4.7}$$

where the energy, $\boldsymbol{E(t)}$, at time $\boldsymbol{t}$ is based on the amplitudes, $\boldsymbol{A(t)}$, of the synthetic or seismic trace within a user defined window, $\boldsymbol{R}$. White and Simm (2003) argue that one of the goals of the seismic-well tie should be to minimize the difference in energy between the synthetic seismogram and real trace. I estimate the energy for the synthetic and seismic trace using Equation 4.7, normalize the results, and weight the LSIM scan.

The parameterization for the LSIM scan weighted by the energy of the synthetic and seismic traces, in Figure 4.8, is the same parameterization used in Figure 4.6; however, the pick estimating the shifts is less oscillatory. Quantitatively, the

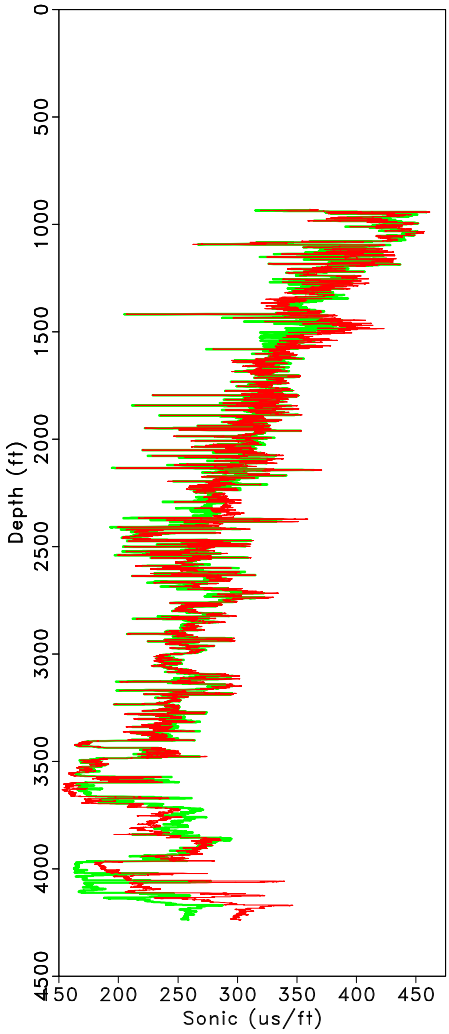

Figure 4.7: Initial sonic log (green). Updated sonic log using the shifts estimated from LSIM (Figure 4.6) to align the synthetic seismogram and real seismic trace (red). Notice that the oscillatory behavior in the shift pick from LSIM results in a significant difference between the original and updated well sonic log. ch04-welltie/../ch02-review/smpltie DT-despike-s1b

correlation coefficient between the synthetic and real traces in the window of 1 to 2.7 seconds is **0.783791**. Although the correlation coefficient from the weighted LSIM scan is less as compared to the unweighted, the velocity update, shown in Figure 4.9, shows significantly less deviation from the initial velocity well log.

This result is useful because I am able to significantly reduce the regularization in the LSIM scan when estimating the shifts for seismic-well ties without introducing unreasonable updates to the velocity log. Additionally, in areas where the well log data or seismic data are noisy, weighting the LSIM scan using the proposed approach ensures high amplitude, hard/soft, reflectors observed in the synthetic seismogram and seismic data are tied while ignoring potentially correlatable noise.

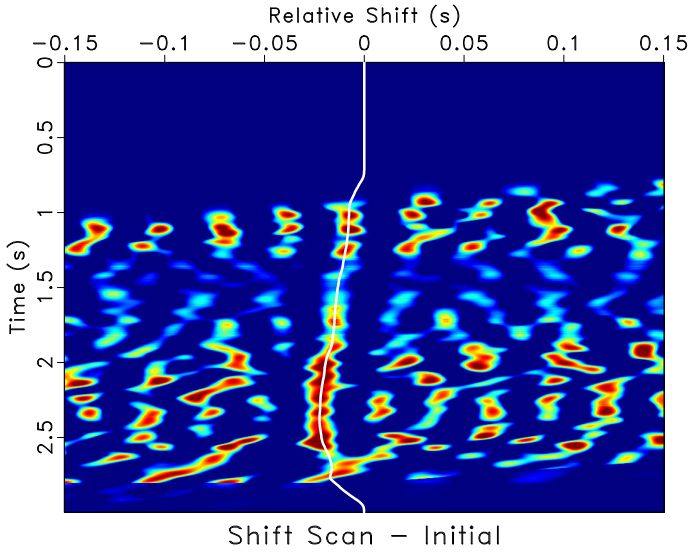

Figure 4.8: Similarity scan between the modeled synthetic seismogram and the real seismic trace weighted by the energy of the synthetic seismogram and seismic trace. Smoothing is reduced by 80% as compared to Figure 4.2. Notice the pick from the similarity scan matches the areas of high similarity. ch04-welltie/../ch02-review/smpltie scanE

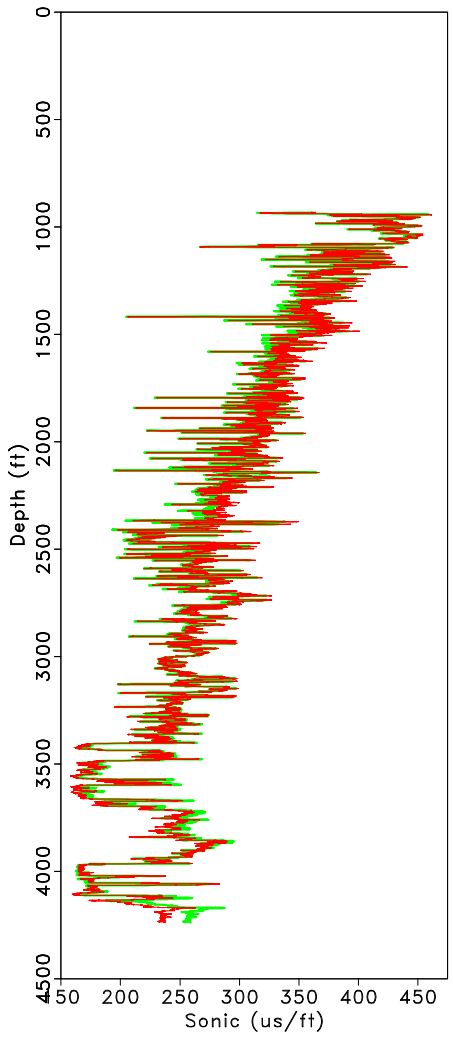

Figure 4.9: Initial sonic log (green). Updated sonic log using the shifts estimated from LSIM (Figure 4.8) to align the synthetic seismogram and real seismic trace (red). ch04-welltie/../ch02-review/smpltie DT-despike-s1E

Teapot Dome dataset seismic-well tie example*

I use 26 wells from the Teapot Dome dataset made available by the U.S. Department of Energy and RMOTC to test the proposed approach as summarized in Table 3.1. First, a complete suite of sonic and density logs are estimated using the approach proposed in Chapter 3. Synthetic seismograms are then modeled independently for each well. White and Simm (2003) argue that modeling synthetic seismograms benefits from blocking or upscaling of the logs. Following their suggestion, I upscale the sonic and density logs to seismic frequencies (Backus, 1962; Marion et al., 1994) and estimate an initial reflectivity series, $\boldsymbol{r(z)}$, from Equation 2.3 in depth assuming no multiples, attenuation or dispersion. It is important to note that stacked thin layers, such as well log measurements, can behave like an anisotropic medium, even if each layer is isotropic (Liner and Fei, 2007). I chose to perform the running average approach, but Liner and Fei (2007) shows that when layer-induced anisotropy develops, the running average approach can produce significant kinematic errors when modeling. After upscaling the logs, each seismic well tie is computed independently by modeling a synthetic seismogram, estimating the shifts using LSIM and computing an updated velocity function. I iterate this process using the updated velocity log to recompute the TDR, reflectivity series and synthetic seimogram.

Prior to performing the seismic-well tie, I need to understand phase variations and distortions introduced during processing and imaging of the seismic data. There are several seismic processing and imaging techniques that adjust the phase in seismic data in an attempt to improve imaging and frequency. The techniques assume the seismic data is minimum phase, which is often an incorrect assumption, and produce

*Parts of this section are published in Bader et al. (2018c).

images that are mixed-phase (Henry, 1997). Because seismic data often contains mixed-phase wavelets (Henry, 2000) and I assume a constant zero-phase wavelet when generating synthetic seismograms, I must adjust the seismic image to zero phase to perform a seismic well tie. Information on phase adjustments applied to the data are not available; however, Harbert (2012) interprets the deepest continuous reflection to be Precambrian basement resulting in a positive amplitude* . As provided by the U.S. Department of Energy and RMOTC, the basement reflection is a negative amplitude. To account for the observed lateral and vertical phase variations, I apply local skewness correction (Fomel and van der Baan, 2014) extended to 3D resulting in a zero phase seismic volume consistent with observations from Harbert (2012).

Additionally, I used Hampson-Russell software to extract a wavelet that is representative of the seismic data's frequency content. The extracted wavelet is shown in Figure 4.10.

Using the phase adjusted seismic data and the wavelet shown in Figure 4.10, I model and perform the seismic-well tie using LSIM. One example of a semiautomatic seismic well tie is shown in Figure 4.11. The synthetic modeled from the original sonic log is compared against the synthetic modeled from a sonic log updated by shifts estimated from four iterations of matching using LSIM and the closest trace from the phase adjusted seismic dataset. The high amplitude reflectors between 0.75 and 1.10 seconds are well-aligned after four iterations of shifts are estimated to update the sonic log.

The initial Backus averaged sonic, updated sonic, and original sonic logs are shown in Figure 4.12(a). I observe that the majority of adjustments to the sonic

*In this thesis, I define a positive amplitude as related to a positive reflection coefficient.

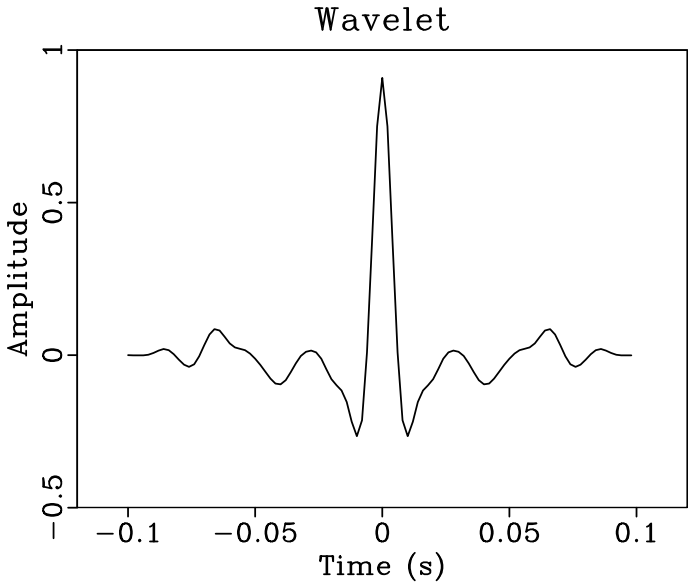

Figure 4.10: Statistical wavelet extracted from the Teapot Dome seismic dataset. ch04-welltie/../interpPaper/logs wavelet200

log occurs between 3500 and 3900 feet. This adjustment can also be observed by comparing the initial and updated TDR's in Figure 4.12(b). The differences between synthetic seismograms modeled from well log data and seismic data are often attributed to either inaccuracies in the seismic phase or seismic migration velocities (White et al., 1998b; Henry, 2000). The bulk shift between initial and final TDR is related to missing shallow velocity section in the well log. The results in Figure 4.12 provide an initial qualitative assessment of a seismic well tie to ensure the estimated shifts do not result in an improbable update to the sonic log. I overlay the modeled and tied synthetic seismogram with the crossline that cuts through the well and observe a good tie with the seismic data, even in the presence of a fault (Figure 4.13).

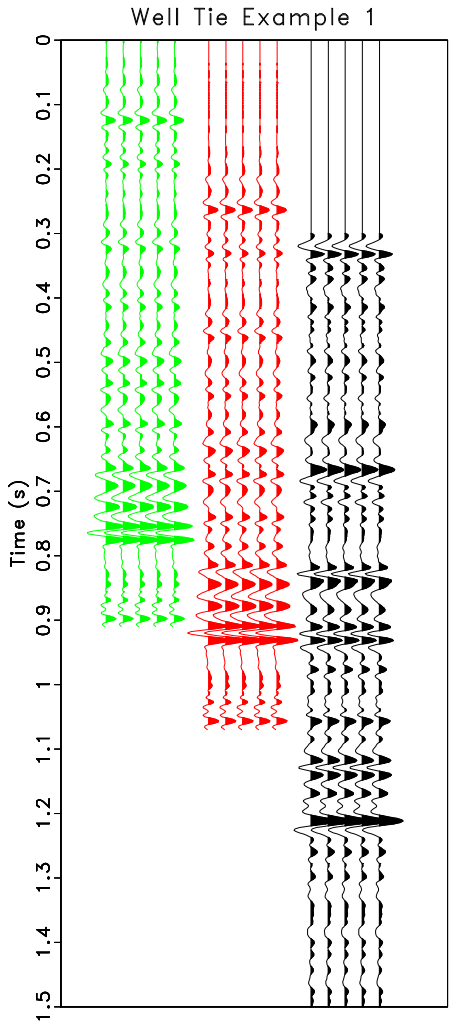

Figure 4.11: Synthetic modeled using the initial sonic log (green). Synthetic modeled using the sonic log updated after four iterations of matching using LSIM to estimate shifts (red). Closest trace to the well location extracted from the phase adjusted seismic data (black). ch04-welltie/../interpPaper/logs synth-p3

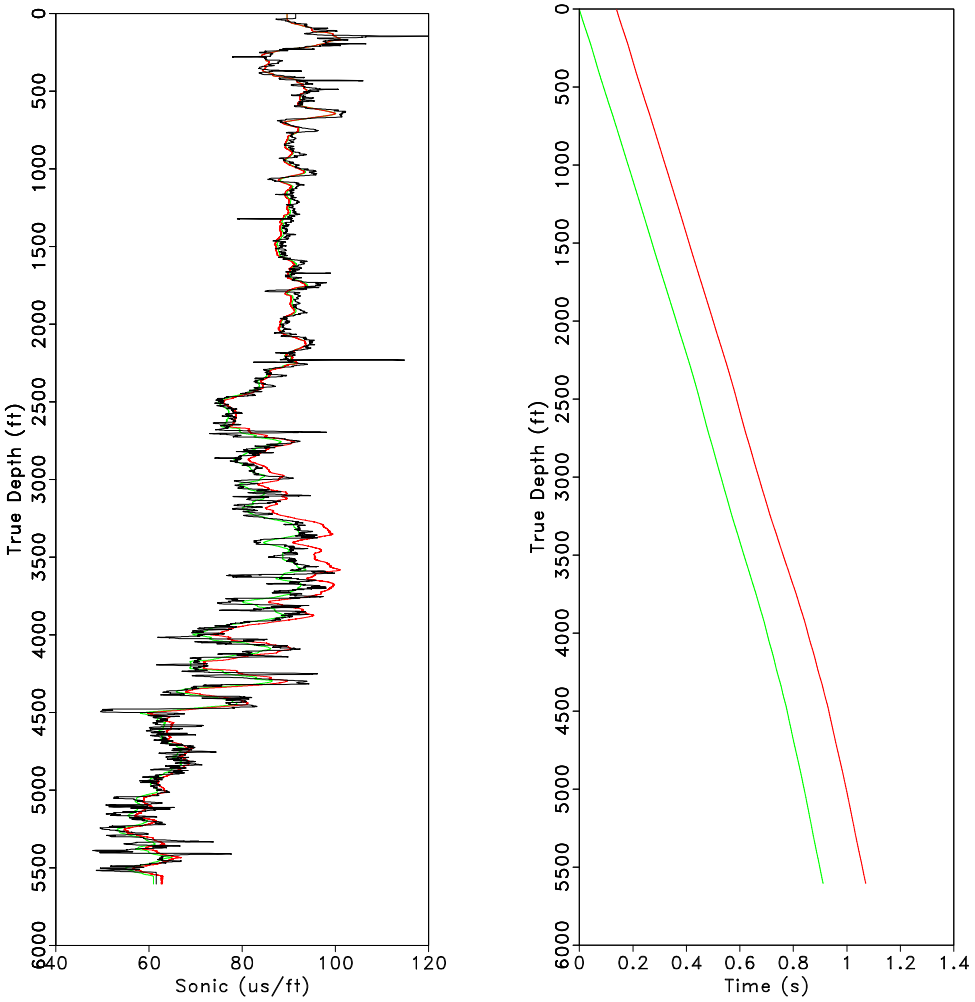

(a) (b)

Figure 4.12: (a) Initial sonic log after Backus averaging (green). Updated sonic log after four iterations of matching using LSIM to estimate shifts (red). Initial sonic log after interpolation of missing data (black). (b) Initial TDR (green). Updated TDR after four iterations of matching using LSIM to estimate shifts (red). ch04-welltie/../interpPaper/logs DTpi3,tdr3

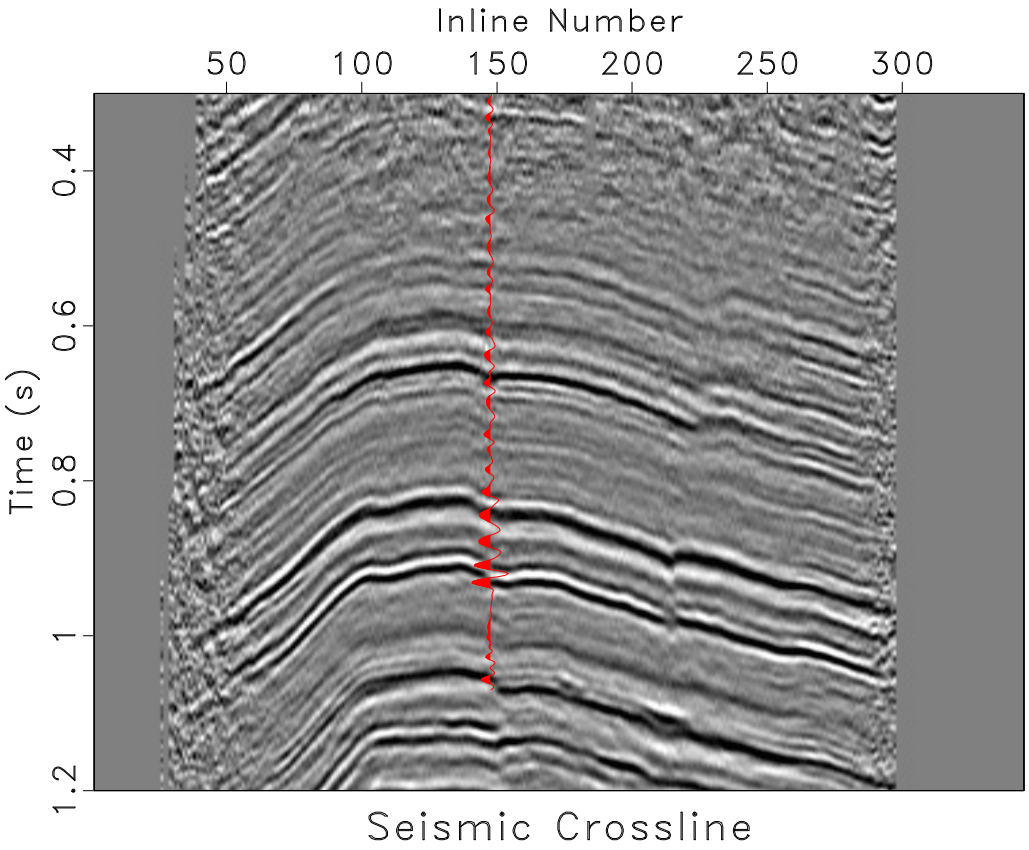

Figure 4.13: Seismic crossline through well in Figures 4.11 and 4.12. I observe a good tie between the modeled synthetic and real seismic data. The sonic and density logs used to model the synthetic are estimated using the proposed approach. ch04-welltie/../interpPaper/logs inline3

Chapter 5

Validation of Technique

To qualitatively assess the result of each seismic well tie, I interpolate well log data from wells along seismic structure. By generating global log-property volumes we can verify the lateral continuity of an log property and perform a blind well test to validate a seismic well tie.

Interpolation using predictive painting

Time dip describes how a seismic event changes from one trace of the next. If available, the dip could be used to interpolate log data along seismic structure and predict an expected log profile in a location with no well log data. Similar to Karimi et al. (2017), I generate log-property volumes by weighting predictive painting. Predictive painting is defined using plane-wave destruction filters that measure the local slope of seismic events (Fomel, 2002). The local slope of seismic events is used to predict one trace from another trace and can be used to interpolate a reference well log through a seismic volume (Fomel, 2010). The interpolation is based on the distance between the reference well and any location in the seismic dataset, as defined in Equation 3.4. The RBF and log property volumes generated from data at each well location are combined to form a single log property volume using the interpolant defined in Equation 2.11.

Computing log property volumes*

We use 26 wells to compute the log property distribution throughout the Teapot Dome seismic survey. Complete density and sonic logs are estimated and tied to the seismic data using the proposed approaches mentioned in the previous sections. Figure 5.1 is a time slice through the 3D seismic volume at 0.72 seconds and shows the location of each well. Figures 5.2(a), 5.2(b), and 5.2(c) show the phase adjusted seismic data and estimated inline and crossline dip using plane wave destruction filters.

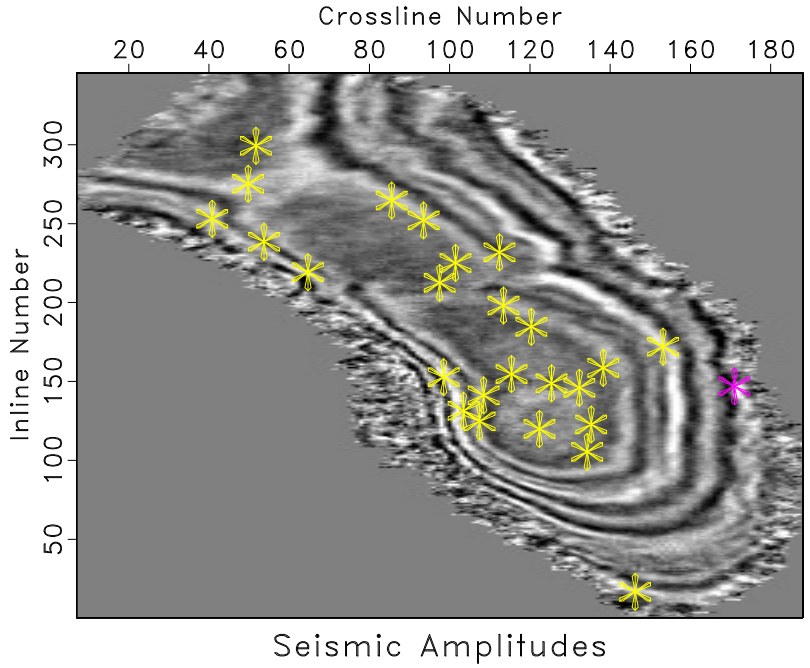

Figure 5.1: Time slice through seismic data at 0.72 seconds. The stars indicate the location of each well. The purple well is used as the reference well for missing log data interpolation. ch05-validation/../interpPaper/logs basemap

The reflection dip is used in the predictive painting algorithm and the RBF

*Parts of this section are published in Bader et al. (2018c).

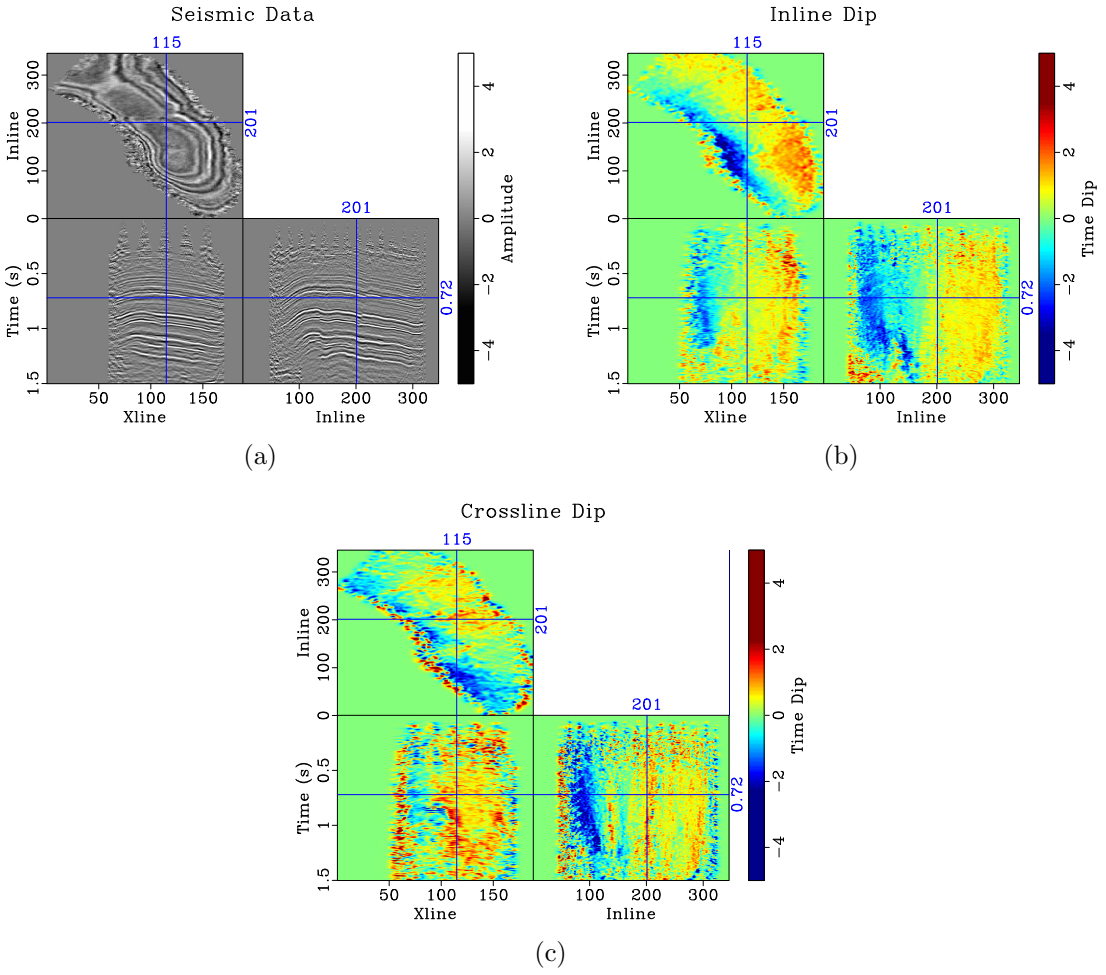

Figure 5.2: (a) Phase adjusted seismic amplitude data. (b) Inline dip and (c) Crossline dip estimated using plane-wave destruction filters. ch05-validation/../interpPaper/logs seismic,dipc1,dipc2

interpolant from Equation 2.11 to generate global log-property volumes. The inputs to the interpolated sonic volume are the original sonic log interpolated to time using a TDR updated from shifts estimated using four iterations of LSIM matching. The results from interpolating sonic logs from 26 well is shown in Figure 5.3(a). We observe reasonable lateral continuity along seismic structure indicating there are no significant misties between well and seismic data. Similar to the interpolated sonic volume, the interpolated density volume shown in Figure 5.3(b) has reasonable lateral continuity along seismic structure and shows little evidence of a mistie. Qualitative interpretation of these results suggest that well ties are laterally consistent.

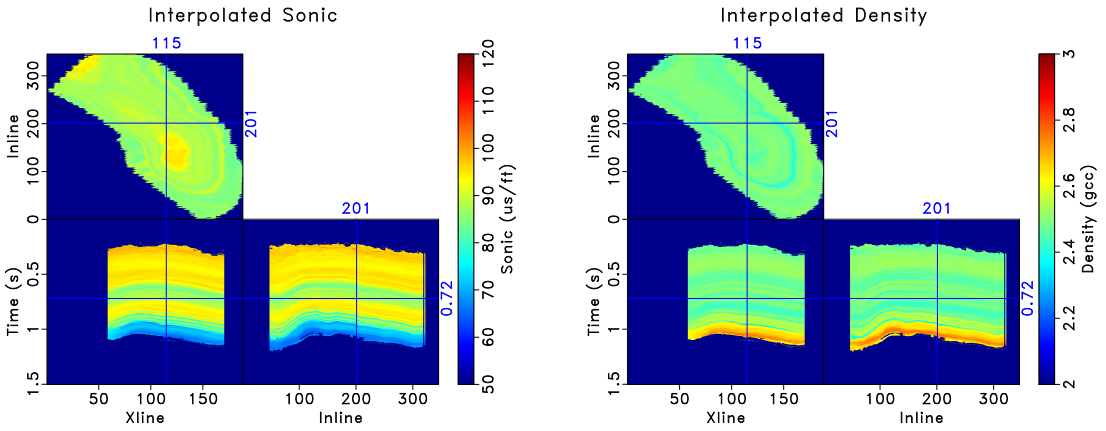

(a) (b)

Figure 5.3: (a) Interpolated sonic and (b) interpolated density based on logs from 26 wells and the interpolant described in Equation 2.11. Note that the interpolated log data follows the seismic structure. ch05-validation/../interpPaper/logs DTvol,RHOBvol

Performing a blind well test

The accuracy of the seismic well ties can be quality checked by removing a well from the interpolation scheme and performing a blind well test. An inconsistent seismic well tie results in misalignment between the predicted and actual log at the

well location. I perform a blind well test using two wells from the 26 well dataset. Results shown in Figure 5.4 indicate a good match between the predicted and actual sonic log at both well locations confirming lateral consistency in seismic well ties.

To understand the accuracy of all seismic well ties, I perform blind well tests at each well using the remaining wells as input. Results of the actual versus predicted sonic at all 26 wells are crossplotted in Figure 5.5.

The results shown in Figure 5.5 indicate the predicted sonic matches reasonably well with the real sonic at all 26 wells giving us confidence that all seismic well ties are consistent and the resulting TDR for each well accurately maps the logs from depth to time.

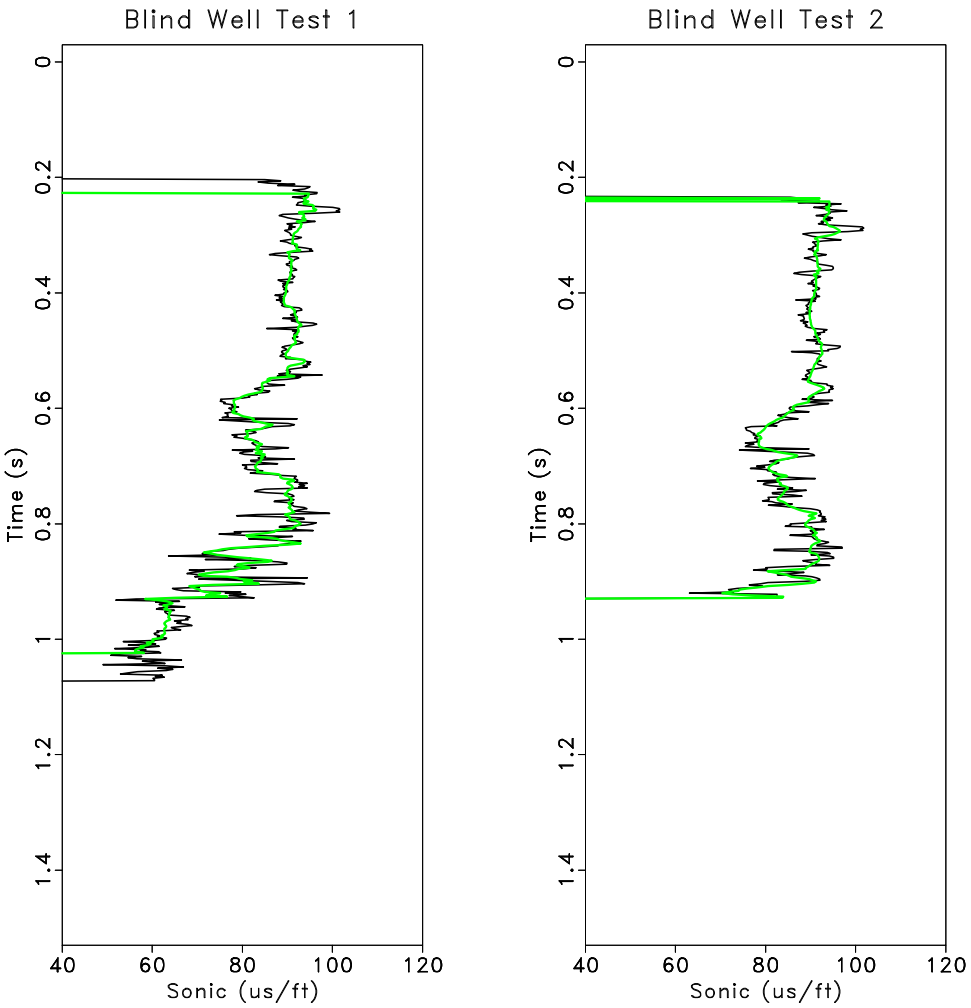

(a) (b)

Figure 5.4: Predicted (green) and actual (black) sonic logs from two different wells using a blind well test. The predicted and actual sonic logs match along the entire length of the well log indicating consistency in seismic well ties. ch05-validation/../interpPaper/logs bwtDT3,bwtDT6

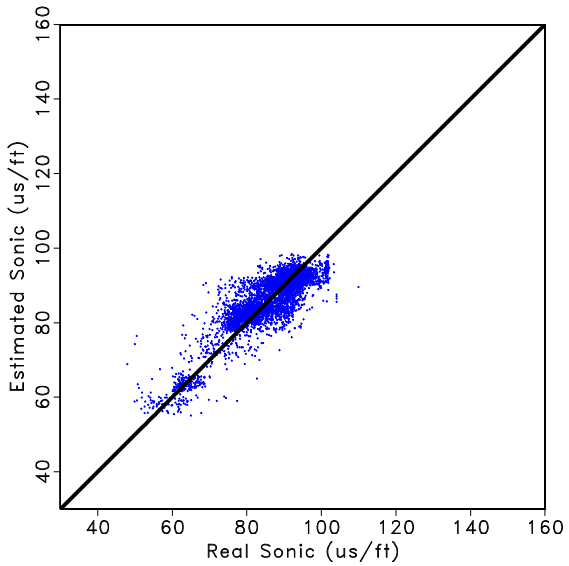

Figure 5.5: Real sonic log cross plotted against the predicted sonic log from the blind well test for all 26 wells. Each blind well test used the remaining 25 wells as input. ch05-validation/../interpPaper/logs xbwt-DT

Chapter 6

Seismic-Well Tie Velocity Update

To understand and reduce the inconsistencies between the migration velocity, well logs, migrated seismic image and modeled synthetic seismogram, I construct several isotropic and anisotropic experiments. In these experiments, I use LSIM to measure the mis-tie between the modeled synthetic and seismic image to provide an understanding of how certain assumptions may impact imaging relative to a modeled synthetic seismogram from well data.

ISOTROPIC SEISMIC-WELL TIE VELOCITY UPDATES USING LOCAL SIMILARITY*

In examples where the media is isotropic, the mis-tie is used to update the migration velocity at the well location using relationships discussed in Chapter 4. The updated velocity profile at each well is interpolated along seismic structure using predictive painting. I test the method on several isotropic synthetic datasets and results indicate that the proposed workflow provides an effective method for incorporating well log data in velocity model building workflows.

Seismic well ties involve matching waveforms from a modeled synthetic seismo-

*Parts of this section are published in Bader et al. (2018a).

gram with a nearby seismic trace (White and Simm, 2003). As previously discussed, several authors note the relationship between the shifts estimated using LSIM and an updated velocity log assuming a TDR defined by Equations 4.1–4.6. Muñoz and Hale (2015), Herrera et al. (2014), and Bader et al. (2018c) use Equation 4.6 to estimate an updated velocity log. Alternatively, if I assume that the migration velocity model is consistent with velocities from logs, I update the migration velocity at the well location based on the proportion of the updated well log velocity to the initial well log velocity:

$$\boldsymbol{v_{mig,1}} = \frac{\boldsymbol{v_1(z)}}{\boldsymbol{v_0(z)}}\boldsymbol{v_{mig,0}}. \tag{6.1}$$

I use predictive painting to spread the updated migration velocity, $\boldsymbol{v_{mig,1}}$, from the wells through the seismic volume. I weight the interpolation based on the distance between the reference well and any location in the seismic dataset using radial basis functions (Karimi et al., 2017).

Using Equations 4.4 and 6.1, the migration velocity is iteratively updated using well-tie velocity updates. The seismic trace from the RTM depth image is stretched to time using the well log velocity profile and compared with the modeled synthetic seismogram from well logs. Figure 6.1 illustrates the workflow I use and is colored based on the data type used in each step.

I test the proposed approach on a simple layered and a more complex isotropic synthetic model. The simple layered model and isotropic synthetic model assume isotropic layers intersect vertical wells; reverse time migration (RTM) is performed to obtain a depth migration image. I assume the following:

1. Seismic image is zero phase

2. Seismic image trace at the well location is stretched to time using the well log velocity

3. Wavelet convolved with well log reflectivity is representative of frequency content of seismic image

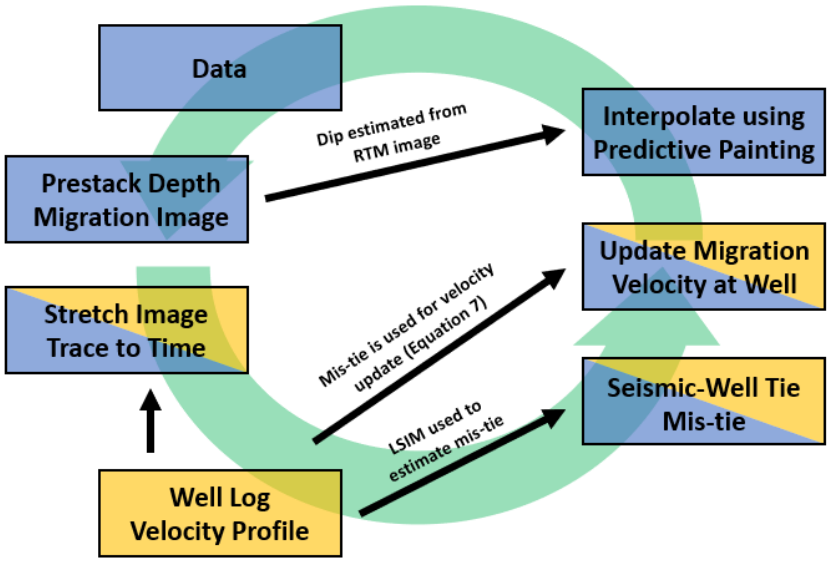

Figure 6.1: Workflow used for seismic-well tie velocity updates. Blue indicates seismic data is used in the step. Yellow indicates well log data is used in the step. Black arrows indicate how the product of one step is used in a different step. ch06-migration/../welltietomo/smpl Capture

Horizontally Layered Isotropic Example

I model data using the true velocity model shown in Figure 6.2(a), and the data migration velocity is shown in Figure 6.2(b). Because each layer is perfectly horizontal, I anticipate that the incorrect migration velocity will cause a discrepancy between the seismic image layer interfaces and the true interfaces from the velocity model.

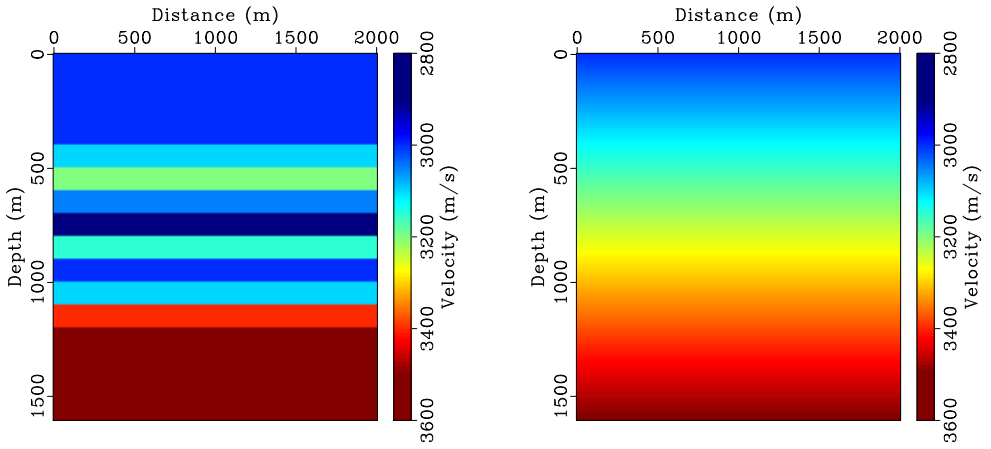

Figure 6.2: (a) True velocity model. (b) Initial migration velocity model. The velocity profile selected for the well tie velocity updates is located at 1000m. ch06-migration/../welltietomo/smpl vels,vel2

A seismic trace is extracted from the seismic image at location 1000m and compared against a modeled synthetic seismogram using a velocity 'well log' from the true velocity mode at 1000m. The seismic-well tie is automatically carried out using LSIM, and a mis-tie function is estimated using the LSIM scan in Figure 6.3. The mis-tie is used to tie the synthetic to the seismic trace in Figure 6.4 indicating the mis-tie function properly related synthetic and seismic traces.

When working with the 'final' seismic image, the mis-tie can be converted to a velocity log update as shown in Figure 6.5(a). Alternatively, I use Equation 6.1 to update the migration velocity as shown in Figure 6.5(b). After ten iterations of well tie updates, I observe that the migration velocity is consistent with the well log velocity in Figure 6.5(c). Note that the updated migration velocity section above 400m and below 1200 is inconsistent with the real velocity as well ties are only possible in between the first and last impedance contrast in the well log data.

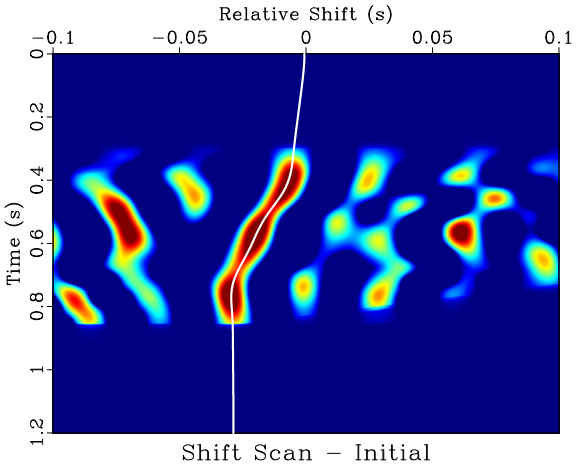

Figure 6.3: Similarity scan using the seismic trace at 1000m, stretched to time using the well log velocity, as the reference trace compared against the synthetic seismogram modeled from the velocity profile extracted at 1000m in Figure 6.2(b). ch06-migration/../welltietomo/smpl scan2

The simple layered model provides the understanding that in isotropic velocity models, the primary reason behind the mis-tie between well log modeled synthetics and seismic data is in the accuracy of the seismic migration velocities. Assuming that the entire mis-tie is related to incorrect vertical positioning of the reflector, the migration velocity model can be effectively updated using Equation 6.1.

The construction of this example is consistent with the assumption that the media is horizontally stratified and the well is vertical; two assumptions I make when generating synthetic seismograms. As a result, incorrect migration velocities move reflectors vertically from proper positioning.

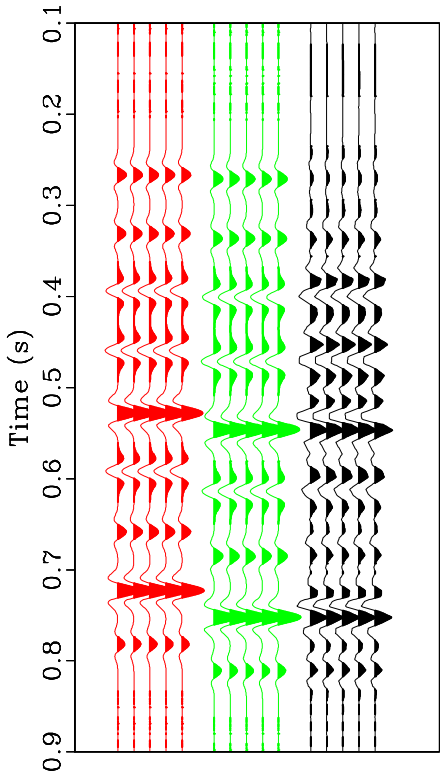

Figure 6.4: Initial synthetic seismogram (red). Synthetic seismogram stretched using the shifts estimated from LSIM scan in Figure 6.3 (green). Seismic trace extracted from RTM image stretched to time (black). ch06-migration/../welltietomo/smpl synthp2

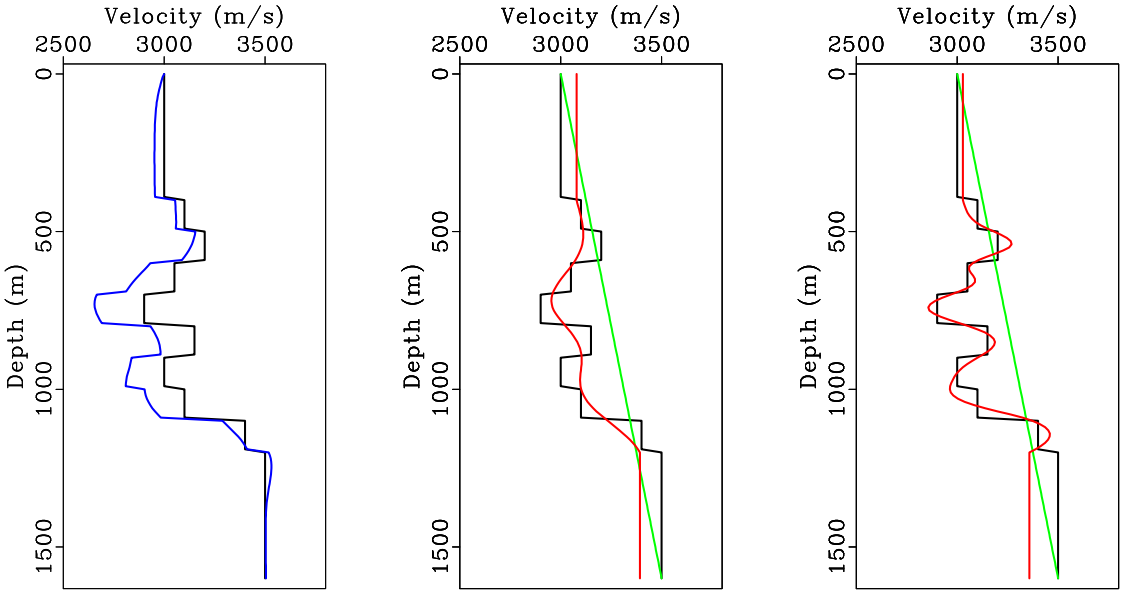

Figure 6.5: Well log velocity profile (black). (a) Common workflow of applying the mis-tie from the synthetic-well tie in Figure 6.4 to update velocity log (blue). (b) Proposed approach of using the mis-tie from the synthetic-well tie in Figure 6.4 to update initial migration velocity (green) at the well location after one iteration (red). (c) Migration velocity profile at the well location after 10 iterations of well tie updates (red) ch06-migration/../welltietomo/smpl velupdate2,itr2,itrfi

Dipping Isotropic Example

In the simple layered model, I assume that the entire mis-tie is related to the vertical positioning of the reflector. However, as pointed out by Bakulin et al. (2010), solving the mis-tie equations along the axis of the well may result in biased estimates of velocities in the presence of dipping layers. Equation 4.6 assumes the entire mis-tie between a common reflector in the modeled synthetic seismogram and real seismic trace is related to a vertical mispositioning of the imaged reflector. In the presence of dipping reflectors, improper migration velocities will move the reflector both vertically and laterally. Consequentially, iteratively updating the migration velocity using Equation 6.1 will likely not converge*.

To account for biased estimates of migration velocity updates due to dipping layers, I propose to migrate the data several times per iteration using perturbed velocity models. I use four percent increments to perturb the model. I then perform the seismic-well tie using each of the resulting seismic images and convert the mis-tie to a migration velocity update for each image. I estimate the migration velocity update for each well location as the semblance weighted average of the velocity updates from each mis-tie. Migration velocity updates are interpolated along seismic structure using predictive painting. Dips are estimated using the image migrated from the mean migration velocity perturbation.

I model data using the true velocity model shown in Figure 6.6(a), and the initial migration velocities are shown Figure 6.7(a). I use a velocity profile from five 'wells' located at 1000m, 2000m, 3000m, 4000m, and 5000m. With each iteration, I

*Results of iteratively updating the migration velocity using Equation 6.1 in the presence of dipping layers are discussed in the Appendix 8.

assume the velocity of the layer between 0m and 400m is known.

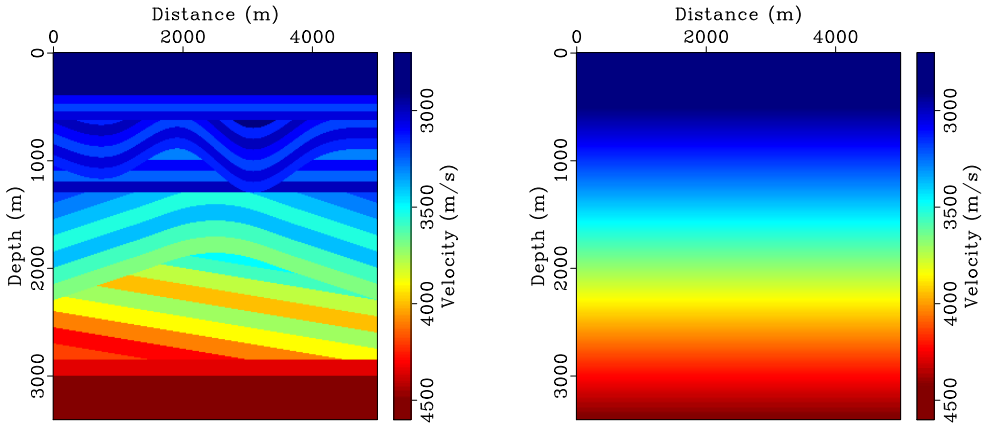

Figure 6.6: (a) True velocity model. (b) One of the initial migration velocity model perturbations for the first iteration. The wells selected for well tie velocity updates are located at 1000m, 2000m, 3000m, 4000m, and 5000m. ch06-migration/../welltietomo/iso vel,vel2-2

The seismic traces at locations 1000m, 2000m, 3000m, 4000m, and 5000m from each seismic image are stretched to time using the true well log velocity and the mis-ties is estimated using local similarity. Using Equation 6.1, I update the migration velocity at each well location. The results of migration velocity updates at well location 3000m for the five initial migration velocity models shown in Figure 6.7(a) are shown in Figure 6.7(b). I spread the information along seismic structures using predictive painting weighted by radial basis functions to generate a new geologically consistent migration velocity model.

I iteratively update the migration velocity model by generating five perturbed migration velocity models at each iteration and estimating the semblance weighted average of the velocity updates from each mis-tie. Each iteration, I reduce the perturbation of the migration velocity models and the smoothing in local similarity.

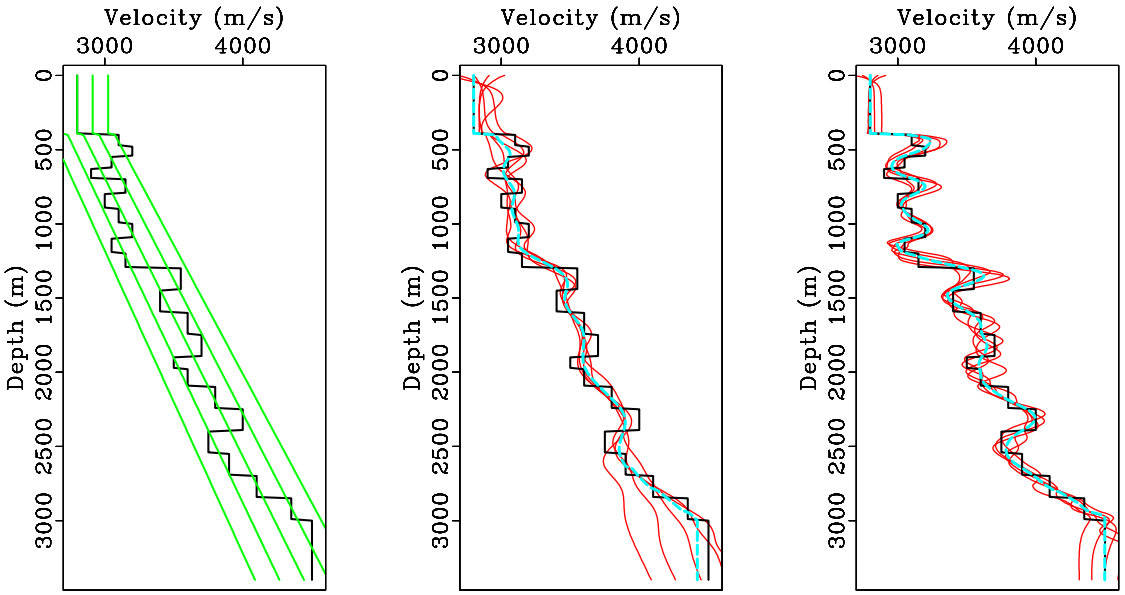

Figure 6.7: True velocity model at well location 3000m (black). (a) Starting migration velocity models with a linearly increasing velocity gradient (green). (b) Migration velocity updates from well tie updates based on the mis-tie between the synthetic seismogram modeled from the well log profile and the seismic image migrated from the five perturbed velocity models (red). Semblance weighted average of the five migration velocity updates (cyan), this result is used for interpolation of the next migration velocity model. (c) Results after six iterations of well tie updates.
ch06-migration/../welltietomo/iso vels2,wellvel2-3,wellvel7-3

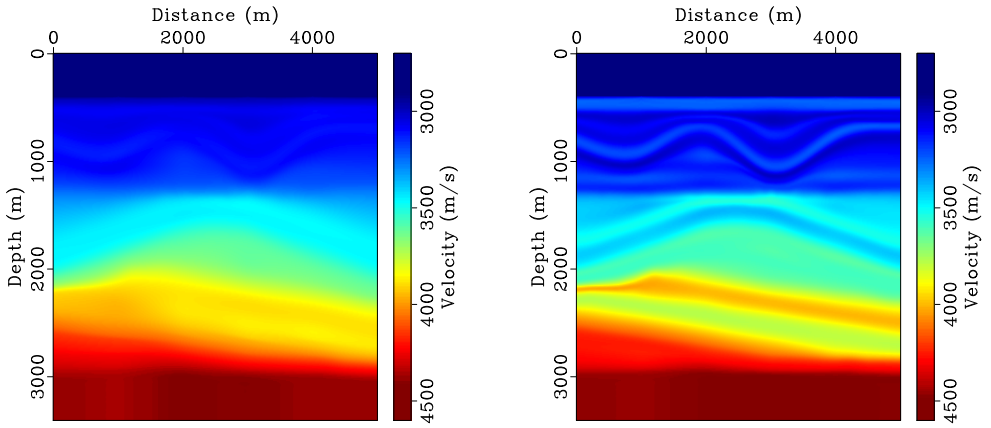

Figure 6.8: (a) Migration velocity model after one iteration and (b) six iterations of well tie velocity updates and weighted interpolation of the updated velocity profile from the wells using predictive painting. ch06-migration/../welltietomo/iso vel3,vel8

Results after six iterations of well tie updates at well location 3000m are shown in Figure 6.7(c). I observe that the semblance weighted average of the velocity updates at this location fits well with the real well log velocity. The migration velocity model after six iterations is shown in Figure 6.8(b) and is reasonably consistent with the real velocity model in Figure 6.6(a).

Figure 6.9(c) is the final depth migrated seismic image using the velocity model in Figure 6.8(b). This result is compared against Figure 6.9(d), the depth migrated seismic image using the real velocity model. Differences in the velocity models result is small differences in reflector positioning.

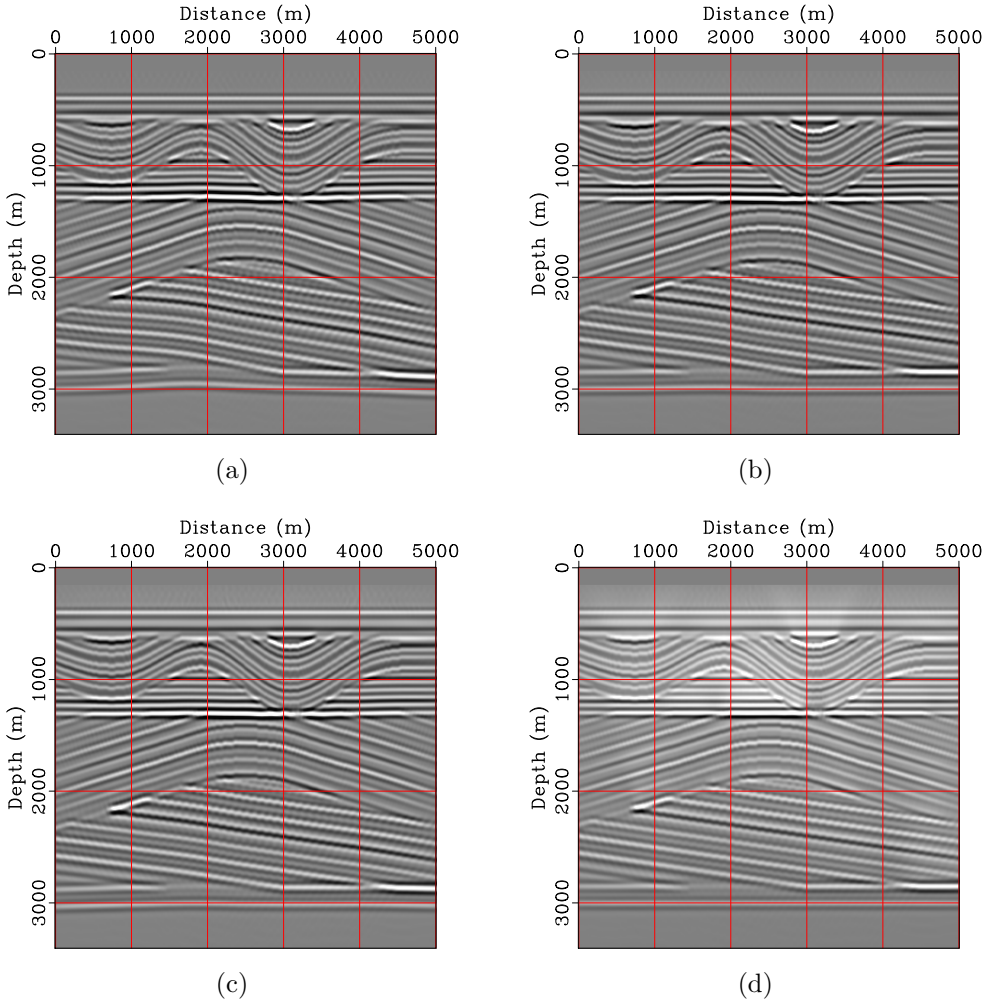

Figure 6.9: (a) Initial RTM image using the migration velocity perturbation shown in Figure 6.6(b). (b) RTM image using the migration velocity perturbation shown in Figure 6.8(a). (c) Final RTM image using the migration velocity shown in Figure 6.8(b) after six iterations. (d) RTM image using the true migration velocity in Figure 6.6(a). ch06-migration/../welltietomo/iso rtm2-2,rtm3-2,rtm8,rtm

Chapter 7

Conclusions

Conventional seismic-well tie workflows are dependent on the availability of sonic and density logs at every well location. Additionally, the seismic-well tie typically involves a subjective and labor-intensive workflow that depends on the interpreter's experience and intuition, making the process non-repeatable and challenging to validate in the presence of multiple well. Using data matching techniques, such as LSIM and predictive painting, I provide an approach of integrating available well log data and seismic data. As indicated by computational examples in this thesis, the proposed approach allows us to predict missing well log data and accurately compute seismic-well ties. It also provides a method to validate the consistency of multiple well ties. Furthermore, the seismic-well tie using LSIM is iterative, with the velocity smoothly updated after each iteration based on the shifts estimated from the LSIM scan. This iterative approach ensures that unrealistic velocity updates are not introduced into the seismic-well tie. The proposed approach is convenient for blind well tests and prediction of well logs properties away from well locations. The final velocity and density models from the Teapot Dome dataset include well log data that have have been previously excluded due to lack of overlapping sonic and density well logs in each well.

The main difference between the proposed workflow and previous/conventional

workflows is that the workflow in this thesis is not limited by specific well logs acquired at every well location and provides a method to perform efficient and verifiably accurate seismic-well ties. Advantages of this approach, as demonstrated in field data examples, is its ability to circumvent challenges with missing well log data whereas conventional approaches, such as empirical equations, provide a well log that may be inconsistent with real data and strongly depends on the availability of certain logs at the well location. The approach has some limitations. In the field data examples reported in this thesis, I assume that the reference type log is representative of the entire stratigraphic column found in other wells; this assumption may cause challenges in plays where rapid stratigraphic variations such as unconformities, channels or clineoforms may be present. Additionally, I did not account for fluid variability in the rocks which can cause different well log responses in the same stratigraphic unit. While fluid substitution may further improve the results, the approach proposed in this thesis provides a reasonable, first-order, approximation of the unknown well logs.

Although the uncertainty of the models compared to the true earth model is not considered in this thesis, one can assume that each constraint added to the proposed workflow (fluid substitution, modeling, etc.) will cast the model into a range of more accurate results. I show, by using field data examples, that the proposed approach is a feasible workflow for overcoming the challenges with the conventional seismic-well tie workflows. Further refinement of the well log information should only improve the results.

Using the relationships from the proposed approaches, I present a novel method to aid in velocity model building using mis-tie between modeled synthetic seismograms from well log data and the seismic image. The proposed approach provides a unique method for incorporating well log data into conventional velocity model build-

ing workflows. Although the proposed workflow is not a substitute for conventional velocity analysis, it may help to reduce nonuniquness in areas of complex stratigraphy or anisotropy. In the approach, I extend the relationship between the shifts estimated from the LSIM scan and the migration velocity model. Because inaccuracies in the migration velocity are directly related to the mis-tie observed in seismic-well ties, this information can be used both to update the migration velocity at the well location and to spread the velocity update throughout the model using predictive painting.

Using the mis-tie between well log and seismic data is not a new idea; however, the implementation described in this thesis provides a constructive method for updating the migration velocity model along every sample of the well log, instead of at discrete tops. In the synthetic examples, I show that the proposed approach may be a useful supplement to conventional velocity model building and migration workflows due to the clear relationship between a seismic-well tie mis-tie and velocity well-log update.

The purpose of integrating seismic and well log data is to provide reservoir characterization that is consistent with all available data and achieves the highest possible resolution. The proposed approach involves including previously ignored wells in seismic well ties and provides a method for verifying the consistency and accuracy of the results. Additionally, previous discussions on seismic-well tie mis-ties fail to provide a clear cause of a well mis-tie and, instead, blamed the result on migration velocities without providing evidence of the claim. The experiments provided in the second part of this thesis provide a clear relationship between well-seismic mis-ties and seismic migration velocities. Further, this relationship can be used to support conventional migration velocity model building workflows.

Future work

Results of the missing well log estimation can be further improved by performing fluid substitution prior to interpolating the missing well log data. The fluid substitution step ensures a consistent response in the logs across the same stratigraphic interval. After estimating missing well logs, it may be challenging to substitute the original fluid content to the predicted well logs without knowledge of the fluid contacts in the reservoir(s). The well log prediction assumes the reference type log contains all stratigraphy found in all wells; in areas with complex stratigraphy that does not correlate between wells, a modeling step to impose an expected log may be an appropriate approach. Additionally, based on the examples presented in this thesis, LSIM accurately estimates the shifts to align post stack seismic data with modeled synthetic seismograms. This approach may be extended to matching prestack seismic data and modeled synthetic data, which may open interesting avenues of research related to amplitude versus offset (AVO) analysis and seismic anisotropy. Prior to performing this analysis, however, I would recommend testing the effects of anisotropy on poststack seismic-well ties. This research may also provide additional insights to the relationship between migration velocity, anisotropy and well logs.

Chapter 8

Appendix

Missing well log data prediction using Bayes' theorem*

Results of missing well log data prediction using Bayes' theorem are further verified by modeling a synthetic seismogram using the available density log with the prior and posterior sonic logs. I use LSIM to estimate the shifts to align the synthetic with the real seismic trace. The seismic well tie using the prior sonic log is shown in Figure 8.1(a) compared against the seismic well tie using the posterior sonic log in Figure 8.1(b). I observe a similar match between 0.85 and 1.1 seconds for both well ties; however, in the shallower section, the waveforms modeled from the posterior sonic log appear more consistent with the seismic data and match more accurately along different reflectors.

*Parts of this section are published in Bader et al. (2018b).

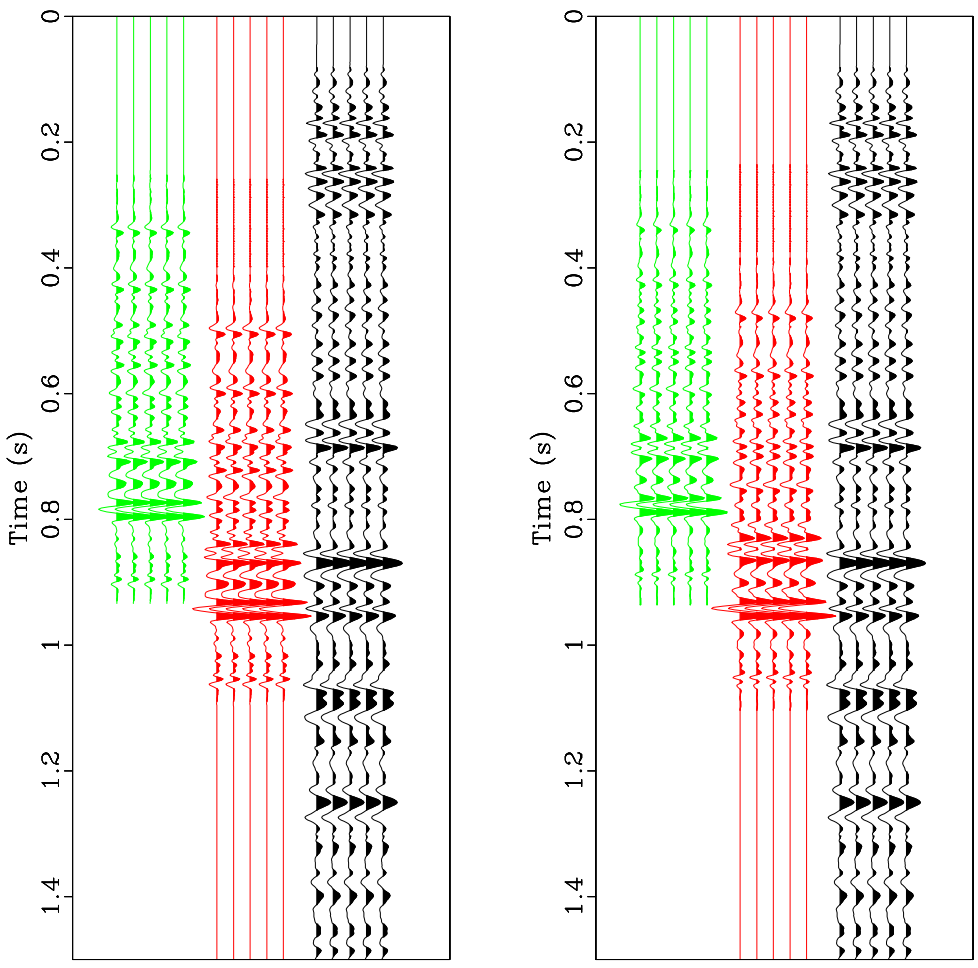

(a) (b)

Figure 8.1: (a) Synthetic seismogram modeled using the a priori sonic log and true density log (green) and tied synthetic seismogram using shifts picked from one iteration of LSIM (red). (b) Synthetic seismogram modeled using the maximum a posteriori sonic log and true density log (green) and tied synthetic seismogram using shifts picked from one iteration of LSIM (red). The reference trace is the seismic trace closest to the well location (black). ch08-appendix/../logbayes/exp synth-prior,synth-bayes

Isotropic seismic-well tie velocity updates using local similarity

I assume that the entire mis-tie is related to the vertical position of the reflector in the presence of dipping reflectors to show the importance of migrating the data several times per iteration using perturbed velocity models at four percent increments as discussed in Chapter 6.

I model data using the true velocity model shown in Figure 8.2(a), and the initial migration velocities are shown Figure 8.2(b). I use a velocity profile from five 'wells' located at 1000m, 2000m, 3000m, 4000m, and 5000m. With each iteration, I assume the velocity of the layer between 0m and 400m is known.

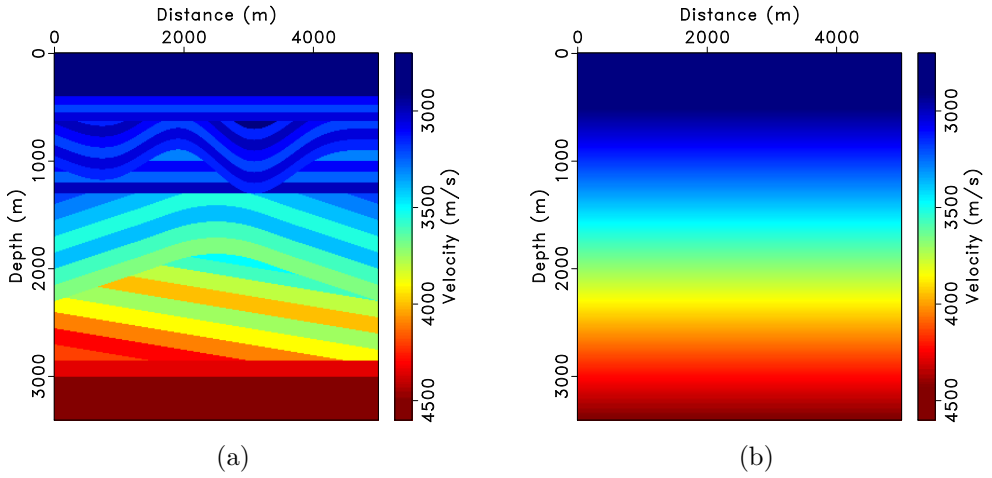

(a) (b)

Figure 8.2: (a) True velocity model. (b) Initial migration velocity model. The wells selected for well tie velocity updates are located at 1000m, 2000m, 3000m, 4000m, and 5000m. ch08-appendix/welltie 8vel,8vel2

The seismic trace at locations 1000m, 2000m, 3000m, 4000m, and 5000m from each seismic image is stretched to time using the true well log velocity and the mis-ties is estimated using local similarity. Using Equation 6.1, I update the migration velocity at each well location. The results of a migration velocity update after one

iteration at well location 3000m is shown in Figure 8.3(b). The information is spread along seismic structures using predictive painting weighted by radial basis functions to generate a new migration velocity model.

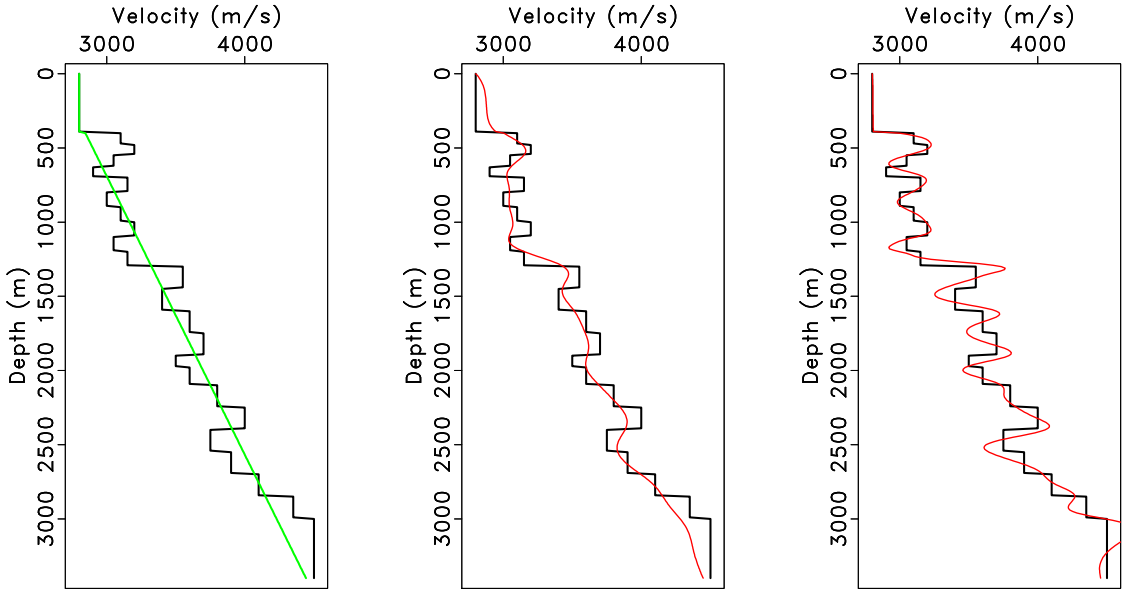

Figure 8.3: True velocity model at well location 3000m (black). (a) Starting migration velocity model with a linearly increasing velocity gradient (green). (b) Migration velocity updates from well tie updates based on the mis-tie between the synthetic seismogram modeled from the well log profile and the seismic image migrated (red). (c) Results after six iterations of well tie velocity updates. ch08-appendix/welltie 8wellvel2,8wellvel2a,8wellvel7

The migration velocity model is iteratively updated. Each iteration, I reduce the smoothing in local similarity. Results after six iterations of well tie updates at well location 3000m are shown in Figure 8.3(c). I observe that the velocity updates are not consistent with the true velocity. Both the velocity value and depth of the updated migration velocity are incorrect indicating that treating the entire mis-tie from the seismic-well tie as a vertical velocity update results in an incorrect migration

velocity model.

This observation is further confirmed by Figure 8.4, where the migration velocity model after six iterations of well tie velocity updates is inconsistent with the true migration velocity model. Additionally, the reflectors in the migrated seismic images (Figure 8.5) are improperly placed vertically and laterally.

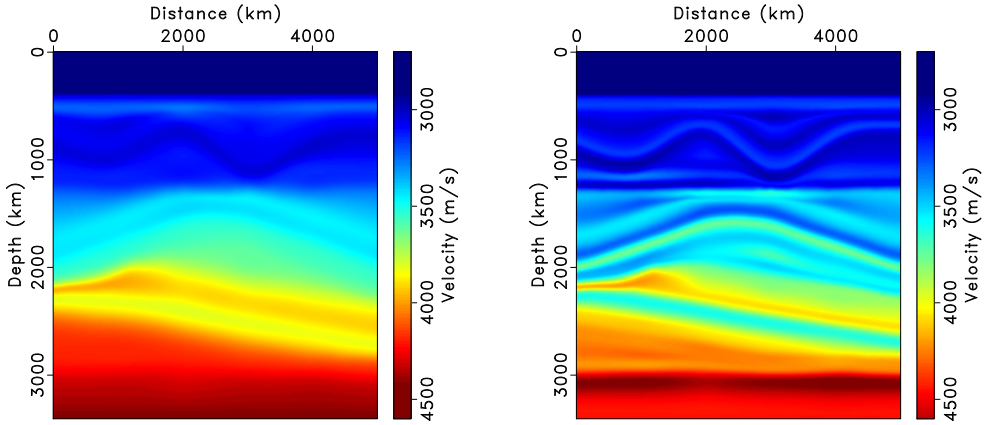

(a) (b)

Figure 8.4: (a) Migration velocity model after one iteration and (b) six iterations of well tie updates and weighted interpolation of the updated velocity profile from the wells using predictive painting. ch08-appendix/welltie 8vel3,8vel8

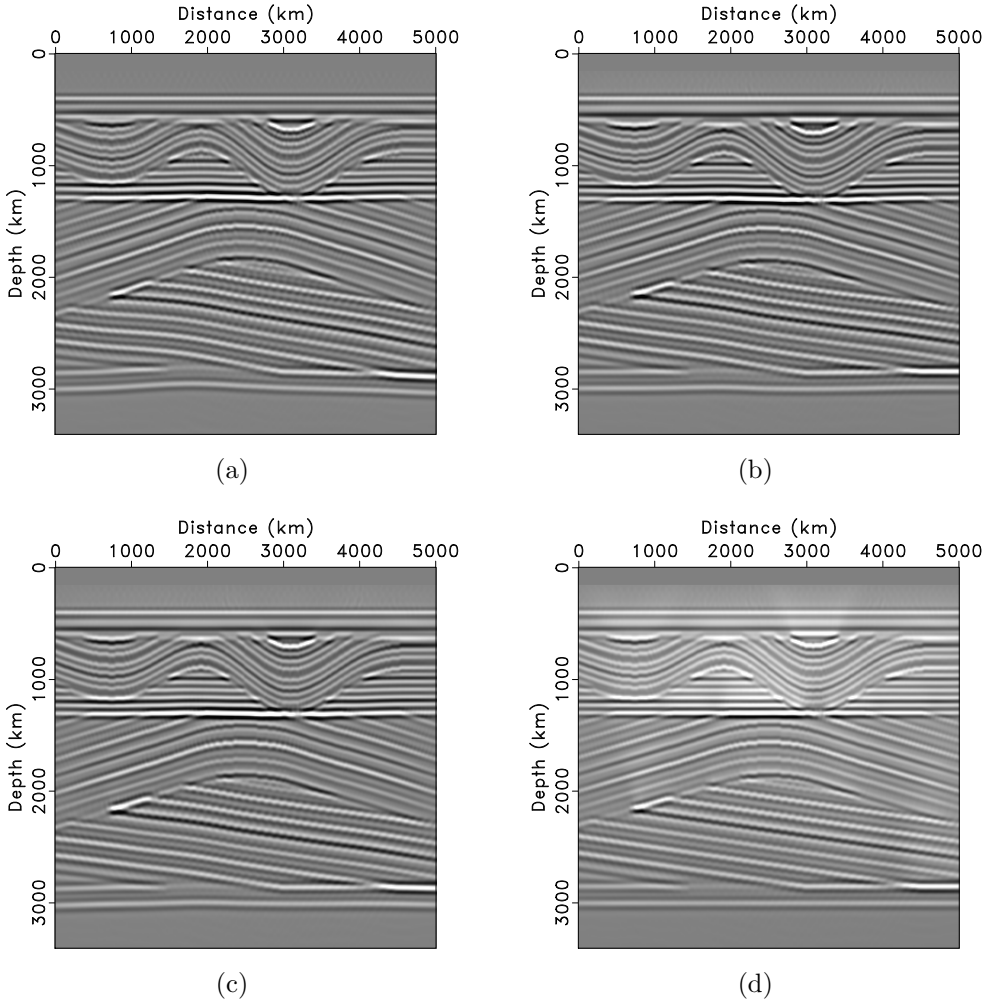

Figure 8.5: (a) Initial RTM image using the migration velocity perturbation shown in Figure 8.2(b). (b) RTM image using the migration velocity perturbation shown in Figure 8.4(a). (c) Final RTM image using the migration velocity shown in Figure 8.4(b) after six iterations. (d) RTM image using the true migration velocity in Figure 8.2(a). ch08-appendix/welltie 8rtm2,8rtm3,8rtm8,8rtm

Bibliography

Aki, K., and P. G. Richards, 2002, Quantitative seismology.

Avseth, P., T. Mukerji, and G. Mavko, 2010, Quantitative seismic interpretation: Applying rock physics tools to reduce interpretation risk: Cambridge university press.

Backus, G. E., 1962, Long-wave elastic anisotropy produced by horizontal layering: Journal of Geophysical Research, **67**, 4427–4440.

Bader, S., S. Fomel, and Z. Xue, 2018a, Using well-seismic mistie to update the velocity model, *in* SEG Technical Program Expanded Abstracts 2018: Society of Exploration Geophysicists, in review.

Bader, S., K. Spikes, and S. Fomel, 2018b, Missing well log data prediction using bayesian approach in the relative geologic time domain, *in* SEG Technical Program Expanded Abstracts 2018: Society of Exploration Geophysicists, in review.

Bader, S., X. Wu, and S. Fomel, 2017, Semiautomatic seismic well ties and log data interpolation, *in* SEG Technical Program Expanded Abstracts 2017: Society of Exploration Geophysicists, 2381–2385.

———, 2018c, Missing log data interpolation and semiautomatic seismic well ties using data matching techniques: Interpretation, moderate revisions.

———, 2018d, Missing well log estimation by multiple well-log correlation: 80th EAGE Conference and Exhibition, Extended Abstracts.

Bakulin, A., M. Woodward, D. Nichols, K. Osypov, and O. Zdraveva, 2010, Localized anisotropic tomography with well information in vti media: Geophysics, **75**, D37–D45.

Berndt, D. J., and J. Clifford, 1994, Using dynamic time warping to find patterns in time series.: KDD workshop, Seattle, WA, 359–370.

Bianco, E., 2014, Geophysical tutorial: Well-tie calculus: The Leading Edge, **33**, 674–677.

Egozi, U., M. Yates, J. Omana, B. V. West, N. Burke, M. Mesa, E. Moreno, J. Checa, M. Martinez, H. Alfonso, et al., 2006, A comprehensive velocity model building approach-cusiana cupiagua sur tti psdm: Presented at the 2006 SEG Annual Meeting, Society of Exploration Geophysicists.

Faust, L. Y., 1953, A velocity function including lithologic variation: Geophysics, **18**, 271–288.

Fomel, S., 2002, Applications of plane-wave destruction filters: Geophysics, **67**, 1946–1960.

———, 2007a, Local seismic attributes: Geophysics, **72**, A29–A33.

———, 2007b, Shaping regularization in geophysical-estimation problems: Geophysics, **72**, R29–R36.

———, 2010, Predictive painting of 3d seismic volumes: Geophysics, **75**, A25–A30.

———, 2016, Fast scattered data gridding, *in* SEG Technical Program Expanded Abstracts 2016: Society of Exploration Geophysicists, 4059–4063.

Fomel, S., and L. Jin, 2009, Time-lapse image registration using the local similarity attribute: Geophysics, **74**, A7–A11.

Fomel, S., and M. van der Baan, 2014, Local skewness attribute as a seismic phase detector: Interpretation, **2**, SA49–SA56.

Gardner, G., L. Gardner, and A. Gregory, 1974, Formation velocity and densitythe diagnostic basics for stratigraphic traps: Geophysics, **39**, 770–780.

Hale, D., 2009, Image-guided blended neighbor interpolation of scattered data, *in*

SEG Technical Program Expanded Abstracts 2009: Society of Exploration Geophysicists, 1127–1131.

———, 2010, Image-guided 3d interpolation of borehole data, *in* SEG Technical Program Expanded Abstracts 2010: Society of Exploration Geophysicists, 1266–1270.

———, 2013, Dynamic warping of seismic images: Geophysics, **78**, S105–S115.

Hampson-Russell, 1999, Theory of the strata program: Technical report, CGGVeritas Hampson-Russell.

Harbert, W., 2012, Rmotc geodatabase: Presented at the , SEG IQ Earth Commitee.

Henry, S., 2000, Pitfalls in synthetics: The Leading Edge, **19**, 604–606.

Henry, S. G., 1997, Catch the (seismic) wavelet: AAPG Explorer (March), 36–38.

Herrera, R. H., S. Fomel, and M. van der Baan, 2014, Automatic approaches for seismic to well tying: Interpretation, **2**, SD9–SD17.

Karimi, P., S. Fomel, and R. Zhang, 2017, Creating detailed subsurface models using predictive image-guided well-log interpolation: Interpretation, **5**, T279–T285.

Kennett, B., 1986, Seismic wave propagation in stratified media: Geophysical Journal International, **86**, 219–220.

Liner, C., and T. Fei, 2007, The backus number: The Leading Edge, **26**, 420–426.

Marion, D., T. Mukerji, and G. Mavko, 1994, Scale effects on velocity dispersion: From ray to effective medium theories in stratified media: Geophysics, **59**, 1613–1619.

Morice, S., J.-C. Puech, and S. Leaney, 2004, Well-driven seismic: 3d data processing solutions from wireline logs and borehole seismic data: First Break, **22**.

Morse, E. L., 2014, Welcome to the revolution: Why shale is the next shale: Foreign Aff., **93**, 3.

Muñoz, A., and D. Hale, 2012, Automatically tying well logs to seismic data: Center for Wave Phenomena, Colorado School of Mines, Golden, CO80401, USA, 253–260.

———, 2015, Automatic simultaneous multiple well ties: Geophysics, **80**, IM45–IM51.

Powell, M. J., 1985, Radial basis function for multivariable interpolation: a review: Presented at the IMA Conference on Algorithms for the Approximation of Functions ans Data, 1985, RMCS.

Rashed, M., 2014, Fifty years of stacking: Acta Geophysica, **62**, 505–528.

Russell, B. H., 1988, Introduction to seismic inversion methods: **2**.

Saggaf, M., and L. Nebrija, 2003, Estimation of missing logs by regularized neural networks: AAPG bulletin, **87**, 1377–1389.

Shi, Y., X. Wu, and S. Fomel, 2017a, Well-log interpolation guided by geologic distance, *in* SEG Technical Program Expanded Abstracts 2017: Society of Exploration Geophysicists, 1939–1944.

Shi, Y., X. Wu, S. Fomel, et al., 2017b, Finding an optimal well-log correlation sequence using coherence-weighted graphs: Presented at the 2017 SEG International Exposition and Annual Meeting, Society of Exploration Geophysicists.

Shier, D. E., et al., 2004, Well log normalization: methods and guidelines: Petrophysics, **45**.

Shuey, R., 1985, A simplification of the zoeppritz equations: Geophysics, **50**, 609–614.

Smith, J. H., 2007, A method for calculating pseudo sonics from e-logs in a clastic geologic setting.

Wheeler, L., and D. Hale, 2014, Simultaneous correlation of multiple well logs, *in* SEG Technical Program Expanded Abstracts 2014: Society of Exploration Geophysicists, 618–622.

White, R., and R. Simm, 2003, Tutorial: Good practice in well ties: First Break, **21**.

White, R., R. Simm, and S. Xu, 1998a, Well tie, fluid substitution and avo modelling: a north sea example: Geophysical Prospecting, **46**, 323–346.

White, R., R. T. Thomas, and A. Castoro, 1998b, Stretch and squeeze-just keeping up appearances?: Presented at the 60th EAGE Conference and Exhibition.

Woodward, M. J., D. Nichols, O. Zdraveva, P. Whitfield, and T. Johns, 2008, A decade of tomography: Geophysics, **73**, VE5–VE11.

Wu, X., 2017, Building 3d subsurface models conforming to seismic structural and stratigraphic features: Geophysics, **82**, IM21–IM30.

Wu, X., and G. Caumon, 2017, Simultaneous multiple well-seismic ties using flattened synthetic and real seismograms: Geophysics, **82**, IM13–IM20.

Wu, X., Y. Shi, S. Fomel, and F. Li, 2017, Incremental correlation of multiple well logs following geologically optimal neighbors, *in* SEG Technical Program Expanded Abstracts 2017: Society of Exploration Geophysicists, 1945–1949.

Vita

Sean Bader grew up in Parker, Colorado and after graduating from Chaparral High School in 2012, Sean attended Colorado School of Mines in Golden, Colorado to pursue a bachelor's degree. After graduating summa cum laude in 2015 with a degree in Geophysics and Geophysical Engineering, Sean began his graduate studies in geophysics at the University of Texas at Austin in 2016. He is a member of the Texas Consortium for Computational Seismology at the Bureau of Economic Geology.

Permanent address: 10593 Oakmoor Circle, Parker, Colorado 80134

This thesis was typeset with LaTeX[†] by the author.

[†]LaTeX is a document preparation system developed by Leslie Lamport as a special version of Donald Knuth's TeX Program.